catalysts

MDPI

Review

Advances in Clean Fuel Ethanol Production from Electro-, Photo- and Photoelectro-Catalytic CO_2 Reduction

Yanfang Song [1], Wei Chen [1,*], Wei Wei [1,2,*] and Yuhan Sun [1,2,3,*]

1 CAS Key Laboratory of Low-Carbon Conversion Science and Engineering, Shanghai Advanced Research Institute, Chinese Academy of Sciences, Shanghai 201210, China; songyf@sari.ac.cn
2 School of Physical Science and Technology, ShanghaiTech University, Shanghai 201210, China
3 Shanghai Institute of Clean Technology, Shanghai 201620, China
* Correspondence: chenw@sari.ac.cn (W.C.); weiwei@sari.ac.cn (W.W.); sunyh@sari.ac.cn (Y.S.); Tel.: +86-21-20350954 (W.C.)

Received: 22 October 2020; Accepted: 3 November 2020; Published: 5 November 2020

Abstract: Using renewable energy to convert CO_2 to a clean fuel ethanol can not only reduce carbon emission through the utilization of CO_2 as feedstock, but also store renewable energy as the widely used chemical and high-energy-density fuel, being considered as a perfect strategy to address current environment and energy issues. Developing efficient electrocatalysts, photocatalysts, and photoelectrocatalysts for CO_2 reduction is the most crucial keystone for achieving this goal. Considerable progresses in CO_2-based ethanol production have been made over the past decades. This review provides the general principles and summarizes the latest advancements in electrocatalytic, photocatalytic and photoelectrocatalytic CO_2 conversion to ethanol. Furthermore, the main challenges and proposed future prospects are illustrated for further developments in clean fuel ethanol production.

Keywords: CO_2 reduction; ethanol; electrolysis; photocatalysis; photoelectrolysis

1. Introduction

With the fast development of the economy and society, the ever-increasing demand for energy all over the world while the limited fossil fuel resources lead to an aggravated energy crisis [1,2]. The huge consumption of fossil fuels causes the constantly accumulating of CO_2 in the atmosphere. By May 2020, the concentration of atmospheric CO_2 reached another record of 412.69 parts per million (ppm) [3], far exceeding the upper safety limit of 350 ppm, which may cause disastrous environmental consequences such as global warming, polar glacier melting, rising sea level, etc. [4]. On the other hand, the renewable energy sources from wind, sun, etc., have been rapidly developed in recent years. Unfortunately, the power from these renewable energy sources cannot be integrated into the electric grid well due to the intrinsic inferiorities of instability and anti-peak-load regulating, resulting in the huge waste and development limitation [5].

An ideal strategy to solve the energy and environmental problems is to convert CO_2 into fuels and value-added chemicals using renewable electricity and/or solar energy. Such a strategy can not only reduce the concentration of atmospheric CO_2 through the utilization of CO_2 as feedstock, but also store renewable energy as fuels and useful chemicals, thus relieving our dependency on fossil fuels [6–8]. Powered by renewable electricity and/or solar energy, CO_2 can be reduced to clean fuels, such as carbon monoxide (CO), methane, formic acid, methanol, ethanol, etc. [9,10]. By contrast, ethanol, a kind of clean and renewable liquid fuel with a higher heating value of −1366.8 kJ·mol^{-1}, is a preferred product. With a higher energy density, easier to store and transport than that of gas products, ethanol has also

been considered as one of the optimal candidate fuels that substitute or supplement fossils in many applications [11]. Ethanol is the most used and largest additive to gasoline, and can be seamlessly accessed by the widest energy infrastructures. Furthermore, ethanol is also an important and widely used common chemical feedstock for organic chemicals and medical disinfectant. Large-scale ethanol production to date is mainly based on the fermentation of agricultural carbohydrates such as cane sugar and cornstarch. However, it seems that nature cannot provide both food and fuel for a still-growing and increasingly energy-hungry world population in the near future Therefore, CO_2 conversion to ethanol driven by renewable energy offers a good alternative (Scheme 1).

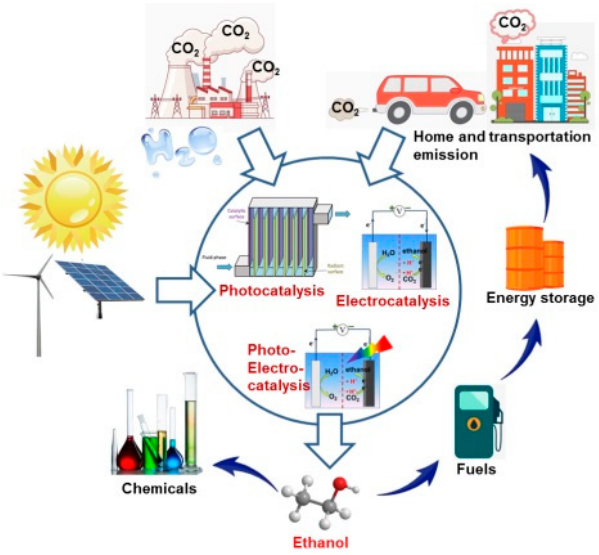

Scheme 1. Schematic illustration of carbon recycling via CO_2-to-ethanol conversion powered by renewable energy sources such as solar and wind.

According to the variety of renewable solar energy assistance, CO_2-to-ethanol conversion can be divided into three major categories: electrocatalytic reduction by an electrolyzer powered by commercial photovoltaic (PV) devices, photocatalytic reduction by an efficient photocatalyst, photoelectrocatalytic reduction by a semiconducting photocathode and an electrolyzer [12]. Over the past decades, numerous efforts have been devoted to researching the three kinds of CO_2 reduction techniques for the production of clean fuel ethanol [13–16]. Different from C_1 products (CO, CH_4, formate, methanol, etc.), the multiple electron–proton transfers involved with ethanol production from CO_2 have been reported with low efficiency due to the kinetic barriers. Typically, multiple electron–proton transfer steps must be orchestrated with their own associated activation energies, thus presenting kinetic barriers to the forward reaction [12]. Therefore, efficient and robust electrocatalysts, photocatalysts and photoelectrocatalysts are required to promote this kinetically sluggish reduction process.

This review will focus on the most-studied catalysts and their corresponding catalytic systems for the reduction of CO_2 to ethanol in the categories of electrochemical, photochemical and photoelectrochemical approaches. Since the catalytic activity and selectivity are mainly determined by the structures and surface states of catalysts as well as the reaction conditions, the second section of this review provides the general principles of electroreduction, photoreduction and photoelectroreduction of CO_2, as well as the theoretical foundation for ethanol production. Lastly, a short prospect is given of the challenges and new directions in the development of efficient CO_2 reduction to solar fuel ethanol.

2. Basic Principles of Clean Fuel Ethanol Production from CO_2

2.1. CO_2 Electroreduction

Electroreduction of CO_2 is commonly carried out in a gas-tight, two-compartment electrolysis cell equipped with a working electrode, a counter electrode and a proton exchange membrane as the separator (Scheme 2A). The membrane was employed to restrict the transport of liquid phase products from the working electrode to the counter electrode where they can be oxidized [17]. Prior to the experiments, the applied gas-tight electrolysis cell should be vacuumed and then purged with CO_2 for 30 min to reach a constant pH value of the electrolyte. The reduction reaction of CO_2 is conducted and measured by cyclic voltammetry and potentiostatic electrolysis at fixed potentials. The gaseous and liquid products are generally quantified by a gas chromatograph and a nuclear magnetic resonance (NMR) spectrometer or a liquid chromatography, respectively. The faradaic efficiency (FE), which is defined as the percentage of electrons consumed for the formation of a given product, can be calculated as follows [18]

$$FE = \frac{\alpha n F}{Q}$$

where α is the quantity of transferred electrons for CO_2 reduction to a given product; n is the number of moles for a desired product; F is the Faraday's constant (96485 C·mol^{-1}) and Q (A·s) is the total quantity of charge passed.

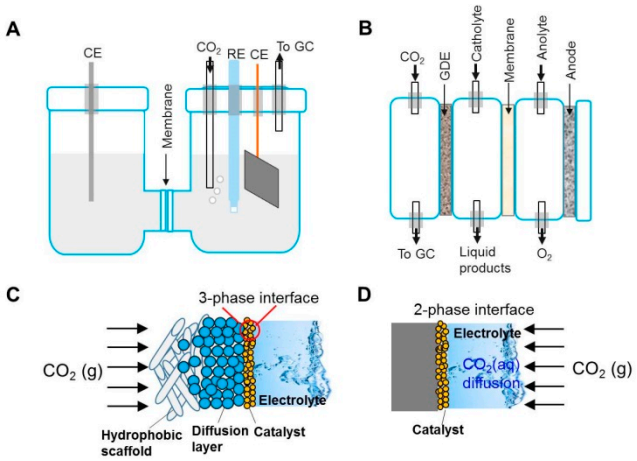

Scheme 2. Illustrations of (**A**) H-cell configuration with a catalyst deposited on a solid substrate, (**B**) flow cell configuration with a catalyst deposited on gas-diffusion electrode (GDE) and a flowing catholyte channel, (**C**) GDE architecture and its 3-phase interface mechanism, (**D**) the working electrode architecture in H-cell and its 2-phase interface mechanism for electrocatalytic CO_2 reduction..

Electroreduction of CO_2 is a multi-step reaction process involving multiple electron transfer, and generally takes place at the electrode/electrolyte interface for the heterogeneous electrocatalysts [19]. It experiences such a process involving three major steps of chemical adsorption of CO_2 on the surface of electrocatalysts, activation of CO_2 to cleave C=O bonds and form C-O or C-H bonds through electron and/or proton transfer, and desorption of products from electrocatalysts surface after configuration rearrangement [18]. The applied electrocatalysts and electrolysis potentials significantly affect the final reduction products that may vary in the carbon compounds of CO, methane, formic acid, ethylene, methanol, ethanol, etc., or a mixture of them. This kind of dependence on electrocatalysts and electrolysis potentials is ascribed to the different thermodynamic equilibrium potentials of these products from CO_2 reduction, as displayed in Table 1 [20]. From the view of thermodynamics, the equilibrium potentials around −0.2 to −0.6 V (versus normal hydrogen electrode (NHE), pH = 7.0) of CO_2 reduction are comparable to that of hydrogen evolution reaction (HER) (−0.41 V, Table 1) [4]. That is why H_2 is the major side-product during CO_2 electroreduction in aqueous

electrolytes. Additionally, the very small differences between the thermodynamic potentials for CO_2 reduction products bring about a challenge to selectively produce the desirable carbon compounds. Actually, the required potentials to drive CO_2 reductions are more negative than the equilibrium ones, leading to the overpotentials [21]. The presence of overpotential originates from the difficult rearrangement of the linear CO_2 molecule to a bent radical anion, which requires enormous energy to occur [22]. Therefore, reducing or even eliminating the overpotentials will facilitate the electroreduction of CO_2.

Table 1. Half-reactions and the corresponding thermodynamic redox potentials of CO_2 reduction to the main products in aqueous solutions [20].

Half-Reactions	E_0 (V vs. NHE)
$CO_2 + 2H^+ + 2e^- = CO + H_2O$	−0.53
$CO_2 + 2H^+ + 2e^- = HCOOH$	−0.61
$CO_2 + 4H^+ + 4e^- = HCHO + H_2O$	−0.48
$CO_2 + 6H^+ + 6e^- = CH_3OH + H_2O$	−0.38
$CO_2 + 8H^+ + 8e^- = CH_4 + 2H_2O$	−0.24
$2CO_2 + 8H^+ + 8e^- = CH_3COOH + H_2O$	−0.29
$2CO_2 + 12H^+ + 12e^- = C_2H_5OH + H_2O$	−0.33
$2H^+ + 2e^- = H_2$	−0.41

Recently, a kind of flow cell using the gas-diffusion electrode (GDE) and flowing catholyte has been developed to accelerate the technology of CO_2 electroreduction toward its envisioned application of neutralizing CO_2 emission on a global scale [23,24]. In this system, the electrolysis cell should consist of three compartments: cathode chamber, anode chamber and gas chamber (Scheme 2B). An ion exchange membrane between cathode chamber and anode chamber is necessary to separate the catholyte and the anolyte. The catalyst is incorporated into electrolyzers on a GDE commonly by drop-casting, spray-coating and in situ growing (self-supporting GDE) [25]. The coated catalyst side of GDE directly contacts the catholyte. Gaseous CO_2 with a certain flow rate passes through the gas chamber at the back side of GDE, and reacts at the catalyst/electrolyte interface, constituting a three-phase boundary (Scheme 2C). This configuration could overcome the mass transfer limitations of two-phase interface and the low solubility of CO_2 in aqueous solution (Scheme 2D). Thus, it enables rapid delivery of CO_2 to the catalyst, resulting in higher or even commercially relevant current densities. Furthermore, this GDE configuration allows the use of more alkaline electrolytes such as KOH, which results in an increased local pH, favoring HER suppression and C_2 (ethanol) production.

2.2. CO_2 Photoreduction

A CO_2 photoreduction system commonly consists of a light source, a photocatalyst, a sacrificial electron donor and a photoreactor that is used as the light absorber [12]. Generally, solar energy can be applied as the energy source for CO_2 conversion [9]. However, CO_2 is optically inert at visible and UV radiation in the wavelengths of 200–900 nm [26]. Thus, a photocatalyst with a suitable band structure is required to promote the CO_2 photoreduction so that the electrons can be excited by sunlight and transfer to CO_2 species adsorbed on the surface of catalysts. The band structure constitutes a conduction band (CB), a valence band (VB) and a bandgap between them with no electron configuration [27]. Accordingly, the CB bottom of the photocatalysts must be more negative than the reduction potentials of CO_2 and its reduced products, while the top of the VB must be more positive than the oxidation potential of sacrificial reagents [4,28]. Thus, the electrons would transfer from the CB of photocatalysts to surface-adsorbed CO_2 species and convert it to solar fuels. As a sacrificial reagent, H_2O is an ideal electron donor and a hydrogen source for the CO_2 photoreduction [29]. However, it can compete with CO_2 photoreduction for the electrons to generate H_2, as shown in HER in Table 1. Therefore, over the semiconductor photocatalysts, H_2O can be not only oxidized to O_2 by trapping the photogenerated holes in the VB, but also reduced to H_2 by catching the photogenerated

electrons in the CB. Commonly, photocatalytic CO_2 reduction is performed in fluidized bed reactor or optical fiber reactor [27]. In fluidized bed reactor [30], the photocatalysts are well dispersed in aqueous solution, thus promoting the contact and reaction between the photocatalysts and water soluble CO_2, but it suffers from the hard separation of products and low light utilization efficiency. By contrast, the photocatalysts coating on the optical fibers in optical fiber reactor [31], considerably improve the illuminated surface area of photocatalysts and light utilization efficiency. Thus, it may be a promising technique to enhance photocatalytic CO_2 reduction efficiency.

The CO_2 photoreduction process generally undergo four major steps: (1) CO_2 molecules are chemically adsorbed on the surface of photocatalysts; (2) under light illumination, the electrons of semiconductor photocatalysts can be excited by photons from VB to CB, leaving an equal number of holes in the VB; (3) the photogenerated electrons are separated from holes and migrate to the photocatalyst surface; (4) the electrons are used to activate and reduce CO_2 into solar fuels, while the holes are consumed by the oxidation of H_2O [32]. According to reactions in Table 1, the photocatalytic CO_2 reduction products are different over various photocatalysts with different CB and VB positions, which is related to the number of electrons and protons (e^-/H^+) involved in reduction reactions. Actually, one electron involved reaction in the reduction of CO_2 is highly unfavorable thermodynamically due to the very negative redox potential of $CO_2 + e^- = CO_2^-$ (−1.90 V vs. NHE) [22]. Therefore, multiple electrons and a corresponding number of protons must be involved in the photocatalytic CO_2 reduction reactions. The clean fuel ethanol can be produced from the CO_2 photoreduction reaction involving twelve electrons and twelve protons, which requires a suitable photocatalyst with multiple electrons easily migrating from a photocatalyst to CO_2. From the point of view of the four photocatalytic steps, a highly active photocatalyst should possess the following characteristics: (1) a large surface area for increasing the adsorption of CO_2 and the surface active sites; (2) a narrow bandgap and proper band positions for utilizing solar energy effectively; (3) a nanostructure favorable for electron transport and improving the separation of photogenerated electron–hole pairs; (4) abundant surface oxygen vacancies for changing the electronic and chemical properties of the semiconductor surfaces and facilitating CO_2 adsorption/activation. Additionally, the co-catalysts are usually attached on the surface of photocatalysts to promote the separation and migration of photo-induced carriers, and effectively lower the reaction energy barrier for CO_2 activation and reduction [33].

2.3. CO_2 Photoelectroreduction

Photoelectrocatalytic reduction of CO_2 is considered as an integration of photocatalytic and electrocatalytic CO_2 reduction, where the solar energy and electricity synergistically promotes the conversion of CO_2 to clean fuels. During the CO_2 photoelectroreduction process, the applied potential facilitates the separation of photogenerated electron–hole pairs in the photocatalytic step, and, in turn, the extra light irradiation could reduce the overpotential in the electrcatalytic step [14]. Photoelectrocatalytic CO_2 reduction system employs semiconductor materials as the photocathodes that can not only used as catalysts, but also as the light harvesting agents. Compared to photocatalysis, much more semiconductors even with a lower CB level than CO_2 redox potential could be function as the photocathodes. Figure 1 shows the CB, VB band edge positions versus an NHE and band gap energies for several common semiconductor photocathodes relative to CO_2 reduction potentials for different products at pH = 7. The CB levels of most of the semiconductors shown in the figure are below the single-electron reduction potential of CO_2 to $CO_2^{\cdot-}$, and only several of them are above the thermodynamic potentials of proton-assisted multi-electron reduction in CO_2.

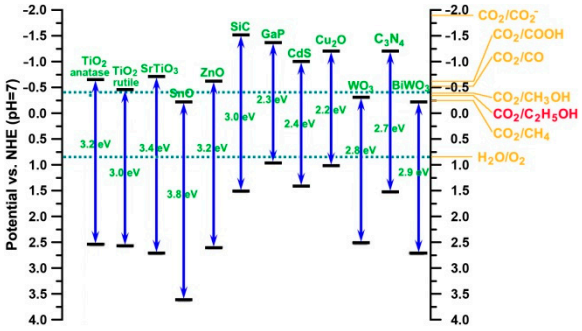

Figure 1. Band structures of some semiconductors with respect to CO_2 reduction potentials for different products at pH = 7.

The reported photoelectrocatalytic CO_2 reduction over electrodes to date mainly contain pure semiconductors, metal-modified semiconductors and semiconductor/metal hybrid catalysts [34–36]. The incorporation of metal species into the semiconductor electrodes has intrigued considerable attention due to their large redox-active surface area, increased light-adsorbing surface area and enhanced electron transport ability. The employed electrode systems in CO_2 photoelectroreduction process can be mainly categorized into two kinds of configurations, those are half-cells with sacrificial reagents donating electrons for oxidation in anode electrode and full-cells with semiconductor photoanodes to compensate electrons for oxidation [14]. In photoelectrochemical reaction cells, the semiconductor electrode is immersed in the electrolyte and is connected to a counter electrode (half-cell) or another semiconductor electrode (full-cell) via an external circuit. When the semiconductor electrode is illuminated under simulated solar light, its electrons can be excited from the VB to CB, leaving an equal number of holes in the VB. Simultaneously, with the aid of extra electric field, the charge accumulating at the interface between semiconductor electrode and electrolyte will give rise to a perturbation of the energy levels of the semiconductor [37]. Inspired by this kind of perturbation, the photogenerated electron–hole pairs are spatially separated and are injected into the electrolyte at the respective electrodes to produce electrochemical CO_2 reduction and water oxidation reactions. Through the conversion of CO_2 to chemicals or fuels, the abundant electricity and solar energy can thus be effectively converted into and stored as chemical energy.

2.4. Mechanisms of Ethanol Production from CO_2

CO_2 reduction is actually a kind of multiple electron–proton-involved reaction whether by electrocatalysis, photocatalysis or photoelectrocatalysis routes. Since CO_2 is a linear molecule and one of the most thermodynamic stable carbon compounds, it demands input energy to activate CO_2. Additionally, CO_2 reduction to clean fuel ethanol using water as the reducing agent to supply protons and electrons, is an uphill reaction with a highly positive change in Gibbs free energy: $2CO_2 + 3H_2O = C_2H_5OH + 3O_2$ ($\Delta G^0 = 1325.3$ KJ·mol^{-1}). Thus, input energy such as electricity or solar energy is required to overcome this reaction barrier. The most energetically demanding and likely key step is the activation of CO_2 with one electron transfer from the catalyst to the lowest unoccupied molecular orbital (LUMO) of CO_2 to form a $CO_2^{\cdot-}$ species [38]. The adsorption of CO_2 onto the catalyst surface can allow for both heterogeneous electron transfer and stabilization of $CO_2^{\cdot-}$ species due to the decreased LUMO level of CO_2 as the molecule bends [39]. Depending on the operating conditions, the type of reductant, the number and potential of the charge carriers involved in the reduction reaction, the following multiple electron–proton transfer steps determine the distribution of products. As shown in Figure 2, CO is formed by two electron–proton transfers through the intermediates of $*CO_2^{\cdot-}$ and *COOH, and is considered as the key intermediate to produce a C_2 product like ethanol [40]. Competing with desorption and loss, a C_1 intermediate like CO should be adsorbed on the catalysts surface firmly enough to persist until a second C_1 intermediate is available for C–C coupling [41]. The surface-bond C_1 intermediate maybe couple with another surface-bond C_1 intermediate or a nearby C_1 intermediate

in the solution [42,43]. The key step of ethanol formation is the C–C bond made at low overpotentials through CO dimerization mediated by electron transfer rendering a $*C_2O_2^-$ intermediate. Indeed, the C–C coupling involves only electron transfer, and proton transfer occurs after the formation of $*C_2O_2^-$ intermediate to stabilize this intermediate for avoiding decoupling [40]. A subsequent seven electron–proton transfers to $*C_2O_2H$ will result in the final production of ethanol. However, moderately adsorbed *CO species can further hydrogenate to *CHO, $*CH_2O$ or $*CH_2$. The C–C bond formation by coulping *CHO, $*CH_2O$ or $*CH_2$ with CO could be more kinetically favorable than CO dimerization for some catalysts [44–46]. Notably, Cu is the only reported metal electrocatalyst that presents the optimal CO binding to the surface, and thus is capable of facilitating these value-added reactions.

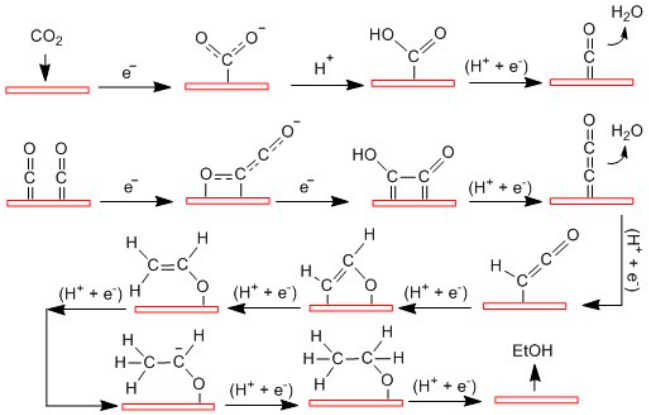

Figure 2. The proposed ethanol formation mechanism of CO_2 reduction. Reproduced with permission [40]. Copyright 2015, American Chemical Society.

Moreover, a radical mechanism was also reported for the ethanol production in photoelectrocatalytic CO_2 reduction process [47]. As shown in Figure 3, the formation of the adsorbed intermediates *CHOO by the first electron and hydrogen radical transfer reaction is the key initial step for CO_2 reduction. The subsequent multiple electron–proton–radical transfer reactions give rise to the formation of $*CH_2O$, an important intermediate for C–C coupling and also for $*CH_3OH$ generation. Thus, the $*CH_2O$ intermediates should be stabilized on the catalyst's surface to some extent, hindering the formation of methanol as a product. Then, the $*CH_3OH$ intermediates can be cleaved into $CH_3^\bullet$ and $OH^\bullet$ radicals. C–C coupling is accomplished though the $CH_3^\bullet$ radicals attacking $*CH_2O$ intermediates in the formation of $*CH_3CH_2O^\bullet$, and ethanol can be finally produced by a further one $H^\bullet$ radical.

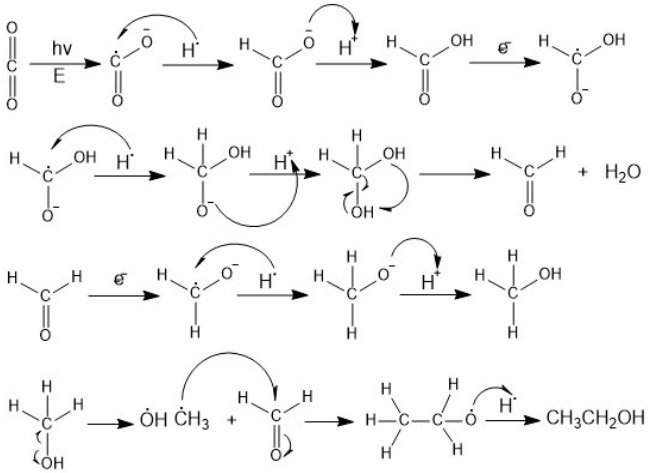

Figure 3. The radical mechanism proposed for ethanol formation by photoelectrocatalytic CO_2 reduction. Reproduced with permission [47]. Copyright 2015, Elsevier.

Although numerous efforts have already been devoted to discover the intermediates and products involved in the CO_2 reduction process, the various proposed mechanisms of ethanol production indicate that more definitive studies are required.

3. The Advances of CO_2 Reduction to Clean Fuel Ethanol

Considering the fact that the linear CO_2 molecule is fully oxidized and extremely stable, it is rather difficult to convert CO_2 into fuels, especially for ethanol production involving multiple electron–protons. Therefore, whether using electricity, sunlight or both of them as input energy, it demands the corresponding specific catalysts to accelerate the CO_2 reduction reaction. Essentially, the performance of CO_2 reduction depends on the properties of the applied catalysts. In the following part, recent important progress in material exploration for CO_2 conversion to ethanol will be discussed in three categories, namely electrocatalysts, photocatalysts and photoelectrocatalysts, as shown in Scheme 3.

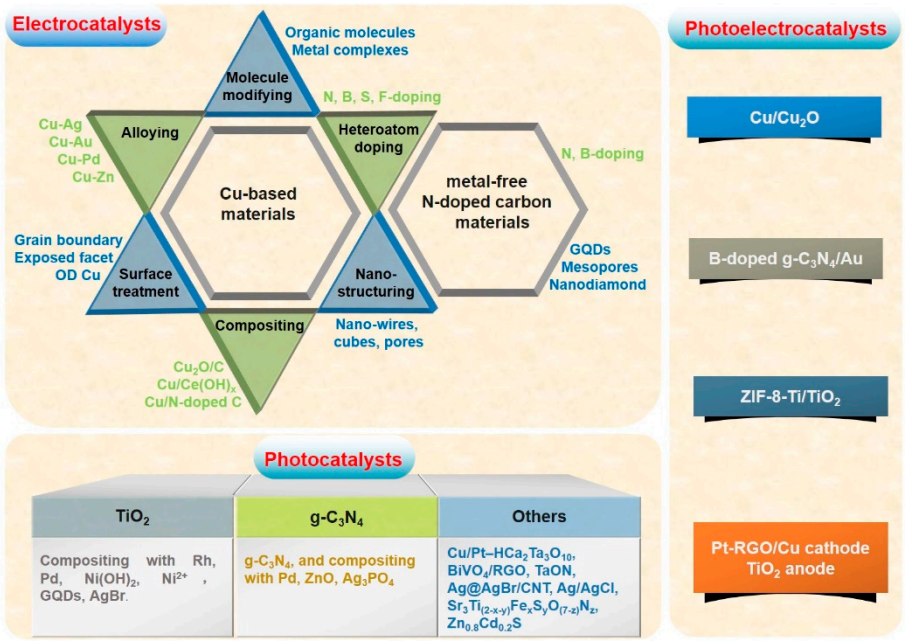

Scheme 3. Illustrations of the catalysts and the corresponding strategies for achieving elctrocatalytic, photocatalytic and photoelectrocatalytic CO_2 conversion into clean fuel ethanol, respectively.

3.1. Electrocatalytic CO_2 Reduction to Ethanol

Since the pioneering work on CO_2 electroreduction to HCOOH over mercury cathodes was reported in 1954 [48], much research has been done on electrocatalytic CO_2 conversion into fuels [10,15,18]. However, studies on the ethanol production from CO_2 electroreduction have increased in the last five years. In this process, theoretically, electrons are released from water oxidation at the anode and travel through an external wire to the catalysts' surface at cathode to reduce CO_2 to various products. The ethanol production is a combination of the oxidation reaction at anode and reduction reaction at cathode involving twelve electron–protons. As the catalysts for CO_2 electroreduction, metals and metallic complexes have been extensively investigated [18,49]. Among these metal-containing catalysts, Cu-based catalysts have been reported as the most promising electrodes that are possibly capable of catalyzing the reduction of CO_2 to clean fuel ethanol [50,51]. The unique catalytic property of Cu originates from its moderate binding energy for CO intermediates, as evidenced by Density functional theory (DFT) calculations. The currently identified Cu-based catalysts those can electroreduce CO_2 to ethanol include modified Cu (morphology, size, facet, doping, organic additives, et al.), Cu-based alloys, Cu/carbon composites and Cu-based metal-organic porous materials (Table 2).

Moreover, metal-free nitrogen-doped carbon materials have also been reported recently to be capable of ethanol production from CO_2.

Table 2. Summary of the main electrocatalysts with the ability to convert CO_2 into ethanol.

Electrocatalyst	Electrolyte	Potential (V vs. RHE)	EtOH FE (%)	Ref.
Cu nanowire (7 μm in length)	0.1 M $KHCO_3$	−1.1	4	[52]
Nanoporous Cu	1 M KOH (flow cell)	−0.67	17	[53]
Oxide-derived Cu foil	0.1 M $CsHCO_3$	−1.0	18	[54]
Electro-redeposited Cu	0.1 M $KHCO_3$	−1.1	12	[55]
Cu nanocubes	0.1 M $KHCO_3$	−1.1	10	[56]
Cu nanocubes with exposed (100) facets	0.25 M $KHCO_3$	−0.95	13	[57]
Grain-boundary-rich Cu	1 M KOH (flow cell)	−1.3	32	[58]
Cu_2O film	0.1 M $KHCO_3$	−0.99	16	[45]
3D dendritic Cu-Cu_2O	0.1 M KCl	−0.4	32	[59]
Multihollow Cu_2O	2 M KOH (flow cell)	−0.61	27	[60]
Cu-on-Cu_3N	0.1 M $KHCO_3$	−0.95	19	[61]
B-doped oxide-derived-Cu	0.1 M $KHCO_3$	−1.05	20	[62]
B-doped Cu	0.1 M KCl	−1.1	27	[63]
Cu_2S-Cu-V core-shell nanoparticles	1 M KOH (flow cell)	−0.92	25	[64]
F-modified Cu	1 M KOH (flow cell)	−0.54	16	[65]
$Ce(OH)_x$-doped-Cu	1 M KOH (flow cell)	−0.7	43	[66]
Polycrystalline Cu electrode with N-tolylpyridinium chloride additive	0.1 M $KHCO_3$	−1.1	31	[67]
Cu electrode with N,N′-ethylene-phenanthrolinium dibromide	0.1 M $KHCO_3$	−1.07	15	[68]
1-octadecanethiol-modified dentritic Cu electrode	0.1 M $CsHCO_3$	−1.1	17	[69]
FeTPP[Cl]-functionalized Cu electrode	1 M $KHCO_3$ (flow cell)	−0.82	41	[70]
$Cu_{63.9}Au_{36.1}$	0.5 M $KHCO_3$	−0.41	12	[71]
$Cu_{55}Ag_{45}$	0.1 M $KHCO_3$	−1.4	25.5	[72]
CuAg alloy wire	1 M KOH (flow cell)	−0.7	25	[73]
CuAg poly	1 M KOH (flow cell)	−0.75	20	[73]
Cu wire	1 M KOH (flow cell)	−0.7	27	[73]
$Cu_{85}Ag_{15}$ foam	0.5 M $KHCO_3$	−1.0	33.7	[74]
CuPd	1 M KOH (flow cell)	−0.75	15	[75]
Cu_4Zn	0.1 M $KHCO_3$	−1.05	29.1	[44]
ZnO@CuO-derived CuZn	1 M KOH (flow cell)	−0.68 V	41.4	[76]
ZnO@CuO-derived CuZn	0.1 M $KHCO_3$	−1.15	32	[76]
Cu_2O nanoparticles/carbon	0.1 M $KHCO_3$	−1.1	12	[77]
Cu nanoparticles/N-doped carbon	0.1 M $KHCO_3$	−1.2	63	[41]
HKUST-1-derived Cu/C	0.1 M $KHCO_3$	−0.5	35	[78]
N-doped porous carbon-supported Cu nanoparticles	0.2 M $KHCO_3$	−1.05	64.6	[79]
N-doped graphene quantum dots	1 M KOH (flow cell)	−0.75	16	[80]
Cylindrical mesoporous N-doped carbon	0.1 M $KHCO_3$	−0.56	77	[81]
Hierarchical porous N-doped carbon	0.1 M $KHCO_3$	−0.56	78	[82]
B, N-co-doped nanodimond	0.1 M $NaHCO_3$	−1.0	93.2	[83]

3.1.1. Modified Cu

The morphology and structure of metallic Cu catalyst significantly affect the product distribution and selectivity of CO_2 reduction. For example, the in situ deposited Cu nanodendrites exhibited increased selectivity toward the formation of ethylene compared to the polycrystalline Cu [84]. It is known that the Cu (111) surfaces preferentially catalyze the methane formation, while the Cu (100) surfaces favor the formation of ethylene [40]. Hence, several strategies, such as controlling morphology, size or the exposed facet of the Cu catalyst, could be employed to attempt to produce the desired ethanol from CO_2 reduction. For instance, Smith and his co-workers prepared Cu nanowire arrays by electroreduction of $Cu(OH)_2$ and CuO nanowire arrays on Cu foil substrates [52]. On these electrocatalysts, the selectivity of hydrocarbon products at a fixed potential can be tuned by altering

the length and density of Cu nanowire which is linked to the increased local pH within the nanowire arrays. Ethanol with a very low FE nearly 4% was produced at −1.1 V vs. RHE on Cu catalyst when the nanowire length increased to 7.3 μm or more. Jiao's group fabricated a nanoporous Cu catalyst through the annealing of $Cu(OH)_2$ nanorods and the electrochemical reduction of the nanoporous CuO [53]. When the porous Cu was integrated into a CO_2 flow cell electrolyzer with 1 M KOH as the electrolyte, it exhibits a high FE of 17% towards ethanol at the current density of 653 $mA{\cdot}cm^{-2}$ and the potential of −0.67 V vs. RHE. This kind of porous structure facilitates rapid gas transport across the electrode–electrolyte interface especially at high current densities. Similarly, the Cu catalysts synthesized by electrochemical oxidation-reduction cycling of Cu foil can electroreduce CO_2 to ethanol with an increased FE up to 18% at −1.0 V vs. RHE in 0.1 M $CsHCO_3$ [54]. Using the sol-gel $Cu_2(OH)_3Cl$ as the precursor, Sargent's group presented an electro-redeposition method to prepare the Cu catalysts with controlled morphologies and oxidation states [55]. At −1.1 V vs. RHE, the electro-redeposited Cu catalyst exhibited a FE of 12% for ethanol product. Loiudice et al. reported the highest FE for ethanol (around 10%) achieved on Cu nanocrystal cubes with 24 nm edge length by tuning nanocrystal spheres (7.5 nm and 27 nm) to nanocrystal cubes (24 nm, 44 nm, and 63 nm) [56]. Overall, the cube-shaped Cu was more intrinsically active than the spheres, and smaller nanocrystals showed higher activity for the same morphology. Additionally, Jiang and co-workers tuned the facet exposure on Cu foil by the metal ion battery cycling method [57]. The 100-cycled Cu nanocube catalyst with exposed (100) facets exhibits a six-fold improvement in C_{2+} to C_1 product ratio compared with the polished Cu foil and an ethanol FE of 13% at −0.95 V vs. RHE.

Additionally, the inclusion of a grain boundary into active sites of Cu-based electrocatalysts has been considered to improve the selectivity of electrocatalytic CO_2 reduction towards multi-carbon products. In a recent report [58], the grain boundary can be controllably grown and enriched in electrodeposited Cu by using the poly (vinylpyrrolidone) additive. The obtained grain-boundary-rich metallic Cu was able to convert CO_2 to ethanol with a high FE of 32% and a partial current density of -45 $mA{\cdot}cm^{-2}$ at −1.3 V vs. RHE in a flow cell, which is superior to the electrodeposited Cu without grain boundary.

Oxide-derived copper (OD-Cu) has been discovered as a simple method to improve the intrinsic catalytic properties towards C_{2+} formation owing to the introduction of Cu^+ species on the surface [45,59,85]. A recent report of thick Cu_2O-film-derived Cu catalysts achieved a higher FE of ethanol at lower overpotential than that on thin OD-Cu films, which can be attributed to the higher content of Cu^+ species [86]. Yeo's group systematically tuned the FE of ethanol by changing the thickness of the deposited Cu_2O overlayers. The highest FE of 16% for ethanol formation was achieved on 3.6 μm film in 0.1 M $KHCO_3$ electrolyte at −0.99 V vs. RHE [45]. These systems have verified the promotion of ethanol production by Cu^+ species. However, the resultant Cu^+ species are prone to being reduced to Cu^0 under CO_2 reduction conditions, especially at the high applied reducing potentials required to produce ethanol [87]. Therefore, research efforts have been done to stabilize the Cu^+ species during CO_2 redution. For instance, a 3D dendritic Cu-Cu_2O oxide composite was developed by in situ reduction in an electrodeposited copper complex on Cu substrate to keep the Cu^+/Cu^0 ratio unchanged during CO_2 reduction reaction, which resulted in a high FE of 32% for ethanol formation [59]. Yu's group recently reported that the nanocavities in the multihollow Cu_2O can confine carbon intermediates formed in situ, which, in turn, covers the local catalyst surface and thereby stabilized Cu^+ species [60]. At the potential of −0.61 V vs. RHE in 2 M KOH, this catalyst yields a maximum ethanol FE of 27% and delivers a high current density of -320 $mA{\cdot}cm^{-2}$ in a flow cell system (Figure 4).

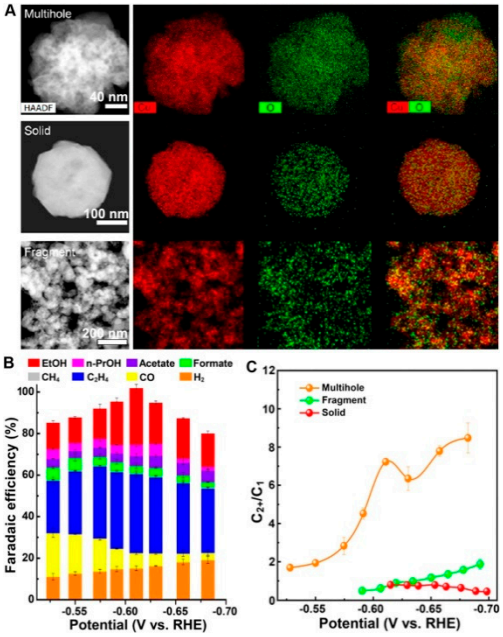

Figure 4. (**A**) TEM-EDX elemental mapping of multihollow, solid and fragment Cu_2O samples. (**B**) FEs of CO_2 reduction major products on multi-hollow Cu_2O. (**C**) C_{2+}/C_1 product selectivity on the three types of catalysts. Reproduced with permission [60]. Copyright 2020, American Chemical Society.

Besides, the incorporation of heteroatoms into catalysts is another efficient approach to stabilized Cu^+ species and promote CO_2 electroreduction. Introducing N into Cu to form Cu_3N, when as the support of Cu catalyst, showed the enhanced FE (around 19%) for ethanol, which results from the stabilized Cu^+ by N in the Cu_3N structure [61]. A B-doped oxide-derived-Cu has been reported to promote C_2 formation with a higher Faradaic effiencicy (20%) than that of OD-Cu (12%), due to the Cu^+ species stabilized by the introduction of B [62]. It has also been reported that B can be used to tune the local electronic structure of Cu with positive valence sites, which results in boosting the ethanol formation with a high FE of 27% at −1.1 V vs. RHE in 0.1 M KCl [63]. By incorporating sulfur atoms in the catalyst core, and Cu vacancies in its shell, Sargent and his co-workers realized Cu_2S-Cu-V core-shell nanoparticles that enhance CO_2 reduction to ethanol with a high FE of 25% in a flow cell [64]. In a recent report, F atoms in the F-modified Cu catalyst facilitate the increase in Cu^+ sites and keeps them unchanged during long-term CO_2 reduction [65]. Thus, a FE of 16% towards ethanol was achieved at -800 mA·cm^{-2} (−0.54 V vs. RHE) in a flow cell system. By increasing surface Cu^+ sites, the modification of F also promotes H_2O activation to *H species, CO adsorption and the hydrogenation of *CO to a *CHO intermediate that can readily undergo coupling.

In order to accelerate H_2O dissociation to *H species and change the H adsorption energy on Cu, Sargent's group reported a complementary approach of hydroxide doping to tune the *H species on Cu [66]. The enhanced *H coverage easily attacks the *HCCOH, forming *HCCHOH, the key intermediate towards ethanol. Hence, the most efficient $Ce(OH)_x$-doped-Cu catalyst exhibits a high ethanol FE of 43% and a partial current density of -128 mA·cm^{-2} in a flow cell.

Bridging homogeneous molecular systems to tune heterogeneous catalysts has been considered a promising approach for the development of new electrodes, combining the advantages of both approaches [88]. When organic molecules or metal complexes are adjacent to heterogeneous active sites, the binding interactions may tune the stability of intermediates, and improve catalytic performance by increasing ethanol FE as well as decreasing overpotential. An good example of this bridge is N-substituted pyridinium additives, which are able to form a deposited film on polycrystalline Cu electrodes upon reduction, tuning the selectivity of ethanol formation [67]. A maximum ethanol FE of 31% was achieved on a polycrystalline Cu electrode with an N-tolylpyridinium chloride additive in a CO_2-saturated 0.1 M $KHCO_3$ electrolyte at −1.1 V vs. RHE. Besides this, a nanostructured Cu

electrode using N,N′-ethylene-phenanthrolinium dibromide as a molecular additive is capable of forming ethanol with a FE of 15% during CO_2 reduction at −1.07 V vs. RHE in 0.1 M $KHCO_3$ [68]. The organic molecule such as 1-octadecanethiol can also be used to modify the dentritic Cu electrode with hydrophobicity [69]. By surpressing HER, this kind of hydropobic electrode attains 17% FE of ethanol at −30 mA·cm^{-2} in 0.1 M $CsHCO_3$ compared to 4% on a hydrophilic equivalent. Another exciting example is the porphyrin-based metallic complex (5,10,15,20-tetraphenyl-21H,23H-porphine iron(III) chloride, FeTPP[Cl]) functionalizing Cu surface, which can provide intermediate-CO-rich local environment that facilitates C-C coupling and steers the reaction pathway towards ethanol [70]. By intergrating it into a flow cell system, the FeTPP[Cl]-functionalized Cu electrode exhibits a CO_2-to-ethanol FE of 41% and a partial current density of −124 mA·cm^{-2} at −0.82 V vs. RHE (Figure 5).

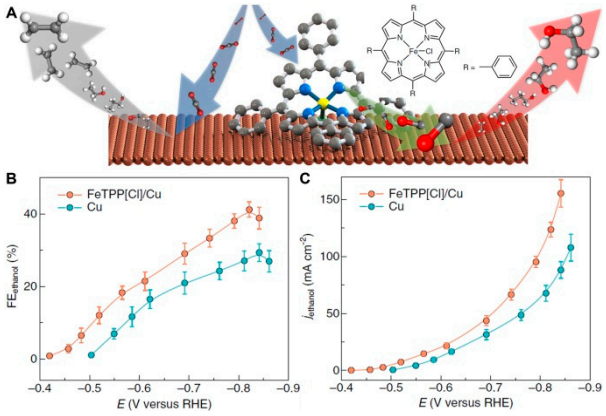

Figure 5. (**A**) Schematic illustration of CO_2-to-ethanol pathway favored by locally generated high-concentration CO on FeTPP[Cl] functionalizing Cu surface, and CO_2-to-ethylene pathway on bare Cu surface. (**B**) Ethanol FE and (**C**) partial current density normalized by geometric area over FeTPP[Cl]/Cu and Cu catalysts at various applied potentials. Reproduced with permission [70]. Copyright 2020, Macmillan Publishers.

3.1.2. Cu Alloy

Coupling another metal with Cu, as a form of interface engieering has been suggested as an effective strategy to break the conventional scaling relationships and tune the binding energy of targered intermediates on Cu surface, thus enhancing the reaction kinetics and selectivity for CO_2 reduction [89,90]. It is promising to design Cu bimetallic electrocatalysts, which will possess intriguing catalytic behavior with respect to that of single-metal electrocatalysts. Those metals (such as Au, Ag, Zn and Pd) with CO as the main product could provide abundant CO to couple with the key intermediate *CO or *CHO on Cu sites for further ethanol formation. For example, $Cu_{63.9}Au_{36.1}$ alloy electrode, which was prepared through electrochemical deposition with a nanoporous Cu film as the template, produced ethanol with an FE of 12% at −0.41 V vs. RHE in 0.5 M $KHCO_3$ [71]. By pulsed electroreduction, ethanol was formed with a maximum FE of 25.5% over $Cu_{55}Ag_{45}$ alloy electrode among the Cu-Ag alloys with different atomic ratios [72]. The key factors for the selective ethanol production from CO_2 are the formation of an oxide layer on Cu and desorption of intermediates on Ag under anodic bias. A kind of high-surface-area CuAg alloy wire was developed by electrodeposition method with 3,5-diamino-1,2,4-triazole (DAT) as an inhibitor [73]. The alloy film containing 6% Ag shows higher activity and selectivity for the electroreduction of CO_2 to ethanol with FE of 25% in comparison to the CuAg poly (20%) without adding the DAT inhibitor, at a cathode potential of −0.7 V vs. RHE and a total current density of −300 mA·cm^{-2}. The origin of the selective ethanol formation is suggested to be the stabilization of Cu_2O overlayer by CuAg wire and the optimal availability of the CO intermediate due to the Ag incorporated in the alloy. Another kind of bimetallic $Cu_{85}Ag_{15}$ foam was synthesized by an additive (citrate)-assisted electrodeposition approach [74]. Such a foam structure enables the phase-segregation of Cu and Ag, and the well-despersed nano-sized Ag in the

Cu matrix. After activation by Cu oxidation/reduction, the $Cu_{85}Ag_{15}$ foam shows high selectivity towards ethanol with an FE of 33.7% at −1.0 V vs. RHE in 0.5 M $KHCO_3$. Bimetallic CuPd catalyst with phase-separated atomic arrangements could achieve a FE of 15% for ethanol formation at −0.75 V vs. RHE in 1 M KOH [75]. While the ordered and disordered Cu-Pd nanoparticles primarily produce CO. This demonstrates that geometric and structural effects may played a more improtant role than electronic effects in determing catalytic performance for various Cu-Pd bimetallic materials. Notably, the FE of CO_2 electroreduction toward ethanol could be tuned by introducing different amounts of Zn to generate an in situ source of mobile CO reactant, and was maximized to 29.1% on Cu_4Zn alloy electrode at −1.05 V vs. RHE in 0.1 M $KHCO_3$ (Figure 6) [44]. Similarily, the bimetallic CuZn catalyst synthesized by in situ electrochemical reduction in ZnO-shell/CuO-core bimetal oxide also shows a preference towards ethanol production with a high FE of 41.4% at −200 mA·cm^{-2} (−0.68 V vs. RHE) in a flow cell, in comparison to 32% at −1.15 V vs. RHE (−31.8 mA·cm^{-2}) in a H-cell [76]. The in-situ-generated CO on Zn sites is believed to combine the adsorbed *CH_3 on Cu sites and form a *$COCH_3$ intermediate, which is exclusively reduced to ethanol. These results indicate that incorporating foreign metals into a Cu matrix can promote or alter the reaction routes of CO_2 reduction and the FE of ethanol formation is greatly dependent on the nanostructures and compositions of Cu-based alloys.

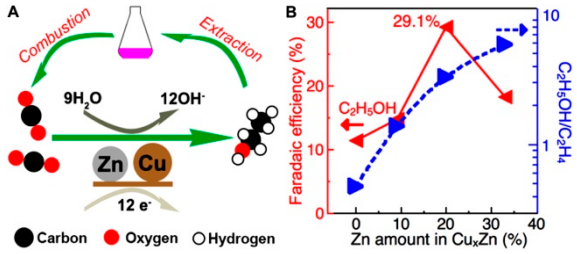

Figure 6. (**A**) Scheme illustration of CO_2 electroreduction process on Cu_xZn alloys. (**B**) The maximum faradaic efficiencies of ethanol and $FE_{ethanol}/FE_{ethylene}$ ratios on different Cu_xZn alloy catalysts. Reproduced with permission [44]. Copyright 2016, American Chemical Society.

3.1.3. Cu/Carbon Composites

Another viable strategy to stabilize the reaction intermediates and promote the ethanol formation is to incorporate porous carbons into Cu catalysts. The large surface area and pore volume of porous carbons will drive the thorough distribution of CO_2 molecules on the surface of catalysts and create abundant active sites for CO_2 conversion. The Cu_2O nanoparticles grown on a carbon support can be transformed into small fragmented nanoparticles during CO_2 electroreduction, which were densely connected to each other [77]. Such a unique morphology is proposed to promote C–C coupling and ethanol formation with FE of 12%. In a recent report, a nitrogen-doped carbon nanospike electrode with electronucleated Cu nanoparticles is shown to acquire a fairly high FE of 63% at −1.2 V vs. RHE in 0.1 M $KHCO_3$ for the electroreduction of CO_2 to ethanol [41]. Subsequently, an oxide-derived Cu/carbon catalyst prepared by a facile carbonization of Cu-based MOF (HKUST-1) at 1100 °C was reported to exhibit highly selective CO_2 reduction to ethanol with a FE of 35% at −0.5 V vs. RHE in 0.1 M $KHCO_3$ [78]. Such intriguing catalytic behaviors originate from the intrinsic activity of Cu and the synergetic interaction between Cu and neighboring porous carbons. In a recent report of N-doped porous carbon-supported Cu nanoparticles [79], the pyridinic N-decorated porous carbon could in situ produce the reactive CO intermediate, which will diffuse to neighboring Cu sites and combine with the C_1 intermediates formed on Cu sites by C–C coupling to produce ethanol. By optimizing the pyridinic N content up to 3.43%, the maximum ethanol FE of 64.6% was achieved at −1.05 V vs. RHE in 0.2 M $KHCO_3$.

3.1.4. Cu MOF

Additionally, Cu-based metal-organic porous materials like HKUST-1, CuAdeAce, CuDTA and CuZnDTA were also reported to electrocatalytically convert CO_2 to ethanol with FEs of 6%, 1%, 3% and 4%, respectively [91]. These catalysts possessing a relatively high surface area, accessibility, and exposure of Cu active sites yield many opportunities for further performance improvements.

3.1.5. N-doped Carbon Materials

Apart from Cu-based catalysts, metal-free nitrogen-doped carbon materials have been reported recently for electroredution of CO_2 to ethanol, and delivered comparable catalytic activities to Cu-based catalysts while possessing better durability. The electronegative nitrogen heteroatoms introduced into the carbon matrixes can increase charge density and convert the inert carbon structures to be highly active. Recently, Ajayan et al. developed nitrogen-doped graphene quantum dots with nanometre-size facilitating the production of ethanol with a FE of 16% at –0.75 V vs. RHE in 1 M KOH [80]. By doping mesoporous carbon with nitrogen, our group has explored a metal-free cylindrical mesoporous nitrogen-doped carbon as a robust catalyst for CO_2 electroreduction, enabling the efficient production of ethanol with an extremely high FE of 77% at −0.56 V vs. RHE in 0.1 M $KHCO_3$ (Figure 7) [81]. The superior electrocatalytic performance was abscribed to the synergy of nitrogen heteratoms and highly uniform cylindrical channel structures that can dramatically boost C–C bond formation in CO_2 electroreduction. Inspired by the potential of tuning the nanostructure of catalyst to acquire C_2 compounds, we further design a class of hierarchical porous N-doped carbon with medium micropores embedded in the channel walls of N-doped ordered mesoporous carbon by a pore-structure-engineering strategy [82]. The embedded medium micropores can not only enrich the exposed active sites (pyridinic and pyrrolic N), but also induce desolvation to accumulate electrolyte ions and enable high local electric potential. Both of them facilitate the activation of CO_2 molecules and the C–C coupling of key intermediates. Therefore, by scaling up the medium micropore content, the production rate of ethanol is increased to 2.3 $mmol \cdot g_{cat}{}^{-1} \cdot h^{-1}$, which is one order of magnitude higher than that of the counterpart without medium microproes (0.2 $mmol \cdot g_{cat}{}^{-1} \cdot h^{-1}$). The FE towards ethanol generation could be maintained at a high value of 78% at −0.56 V vs. RHE. In another exciting example, boron and nitrogen co-doped nanodimond was reported for selective reduction of CO_2 to ethanol with a maximum FE of 93.2% at −1.0 V vs. RHE in 0.1 M $NaHCO_3$ [83]. The synegic effect of boron and nitrogen codoping and fine balance between nitrogen content and H_2 evolution potential drives the highly selective ethanol formation. These results open new insight into electrochemical conversion of CO_2 to clean fuel ethanol.

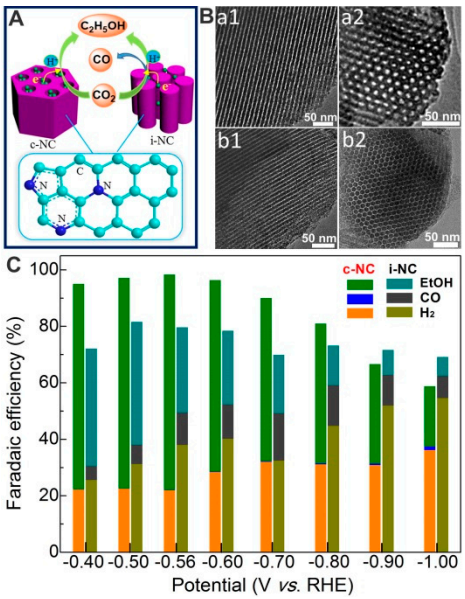

Figure 7. (**A**) Illustration of cylindrical mesoporous nitrogen-doped carbon (c-NC) and the inverse mesoporous N-doped carbon (i-NC) for CO_2 electroreduction. (**B**) TEM images of (a1,a2) c-NC and (b1,b2) i-NC viewed along (a1,b1) (110) and (a2,b2) (100) directions. (**C**) FEs of CO_2 electroreduction products over c-NC and i-NC catalysts at various applied potentials. Reproduced with permission [81]. Copyright 2017, Wiley.

3.2. *Photocatalytic CO_2 Reduction to Ethanol*

Photocatalytic CO_2 reduction has been paid consistent attention for several decades based on the utilization of solar energy and the concept of artificial photosynthesis [92–94]. During the reduction process of CO_2, photocatalysts play a key role in lowering the potential of the electron-proton transfer reaction and the eventual catalytic performance. To date, many kinds of semiconductors have been employed as the photocatalysts for CO_2 reduction to solar fuels [95,96]. However, very few semiconductors like TiO_2 and graphitic carbon nitride (g-C_3N_4) can photocatalyze the ethanol formation.

3.2.1. TiO_2

Actually, TiO_2 is considered the most appropriate candidate of photocatalysts due to its comparable conduction band energy ($E_{cb} \approx -0.5$ eV vs. NHE at pH = 7 as shown in Figure 1) to the reduction potentials of CO_2 (Reaction (1)–(7) in Table 1). However, it has yielded low CO_2 conversion rates to date, and mainly C_1 products of methane and methanol. For the sake of improving catalytic activity and producing ethanol, the incorporating strategies with metals, nonmetals and photosensitive materials have been adopted to modify TiO_2. For example, Rh and Pd nanowires with high density of grain boundaries were in situ grown on TiO_2 nanosheets, acting as the cocatalysts to enhance photocatalytic CO_2 reduction performance [97]. The TiO_2-Rh long nanowires and TiO_2-Pd nanowires composites catalyzed CO_2 reduction to ethanol with an average production rate of 12.1 and 13 $\mu mol \cdot^{-1} \cdot h^{-1}$, respectively, during the 4 h reaction under UV light ($\lambda < 400$ nm). Depositing $Ni(OH)_2$ nanosheets onto TiO_2 nanofibers could enhance charge separation efficiency and CO_2 capture capacity [98]. With 15 wt% $Ni(OH)_2$ loaded, 0.37 $\mu mol \cdot g^{-1} \cdot h^{-1}$ of ethanol was achieved over $TiO_2/Ni(OH)_2$ hybrid catalyst. In another case, the incorporation of matrix facilitated the effective charge separation and CO_2 reduction, in which the average production rate of ethanol was maximized to 13.2 $\mu mol \cdot g^{-1} \cdot h^{-1}$ on 1.5wt%Ni^{2+}-TiO_2 during 4 h of UV light irradiation [99]. Graphene quantum dots (GQDs) were combined with vanadium-doped TiO_2 (V-TiO_2) to effectively separate photogenerated electrons and holes, and 5%GQDs/V-TiO_2 exhibited the best photocatalytic activity with an ethanol production rate of 5.65 $\mu mol\ g^{-1}\ h^{-1}$ under solar spectrum irradiation (Figure 8) [100]. The photosensitive AgBr with a

narrow band gap was coupled with TiO_2 to improve the visible light activity, and the 23.2% AgBr/TiO_2 composite showed a relatively high ethanol yield of 13.28 μmol g^{-1} h^{-1} under visible-light irradiation for 5 h [101].

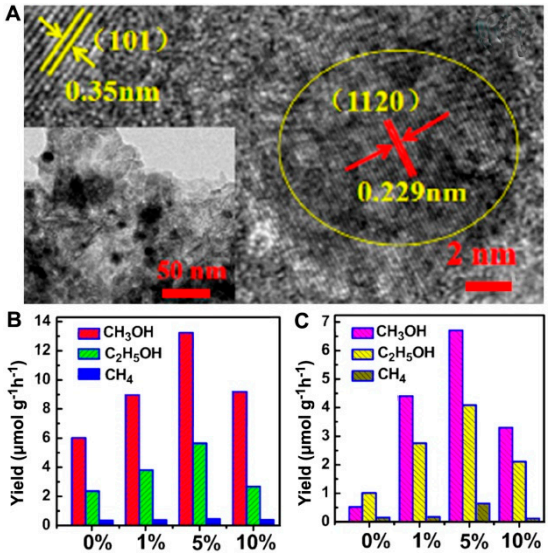

Figure 8. (**A**) HRTEM image of 5%GQDs/V-TiO_2. The yields of methanol, ethanol and methane (**B**) under solar spectrum irradiation and (**C**) under visible light irradiation (λ ≥ 420 nm) on GQDs/V-TiO_2 catalysts with different GQD contents. Reproduced with permission [100]. Copyright 2016, American Chemical Society.

3.2.2. G-C_3N_4

As a novel nonmetallic semiconductor, g-C_3N_4 with a moderate band gap (E_g = 2.7 eV, as shown in Figure 1) has attracted significant attention in photocatalytic CO_2 reduction due to its high stability and responsiveness to visible light. It can be synthesized through the pyrolysis of some nitrogen-rich organic precursors, such as urea and melamine. The g-C_3N_4 derived from urea (u-g-C_3N_4) possessed a mesoporous flake-like structure with a larger surface area and photocatalyzed CO_2 reduction to ethanol in a yield of 4.5 μmol·g^{-1}·h^{-1} with methanol as a co-product under visible-light irradiation for 12 h (Figure 9) [102], while the g-C_3N_4 derived from melamine (m-g-C_3N_4) without porous structure could exclusively yield ethanol at a lower rate of 3.6 μmol·g^{-1}·h^{-1}. The above-mentioned different photocatalytic activities and selectivities for the formation of ethanol are possibly due to the differences in the crystallinity and microstructure of u-g-C_3N_4 and m-g-C_3N_4. The non-porous structure of m-g-C_3N_4 may not favor the fast exchange of the formed *OCH_3 or CH_3OH, thus probably promoting the dimerization of *OCH_3 to form ethanol. Moreover, much effort has been devoted to improving the photocatalytic activity of g-C_3N_4 via the combination with other semiconductors. For example, ZnO with a negative conduction band potential of −0.44 eV was coupled with g-C_3N_4 by an impregnation method to generate ZnO/g-C_3N_4 composite photocatalyst [103]. Although the CO_2 conversion rate was considerably enhanced over the optimal ZnO/g-C_3N_4 composite, the ethanol yield was still as low as 1.5 μmol·g^{-1}·h^{-1} under simulated sunlight irradiation. Meanwhile, the Ag_3PO_4/g-C_3N_4 composite photocatalyst was also reported to significantly improve the CO_2 conversion rate, but exhibit a low ethanol yield of 1.3 μmol·g^{-1}·h^{-1} under simulated sunlight irradiation [104]. When the two-dimensional g-C_3N_4 nanosheets with few-layer thickness were used as the support of Pd to ensure equivalent charge migrations to various Pd facets, the selectivity of CO_2 photoreduction to ethanol strongly depends on the shapes of Pd nanocrystals on the C_3N_4 nanosheets [105]. The optimal ethanol production rate was achieved on Pd nanotetrahedrons loaded on g-C_3N_4 nanosheets with a Pd loading of 5.8 wt%, though the value only arrived at 2.18 μmol·g^{-1}·h^{-1}. Therefore, it still remains challenging to selectively photocatalyze CO_2 reduction to ethanol over g-C_3N_4.

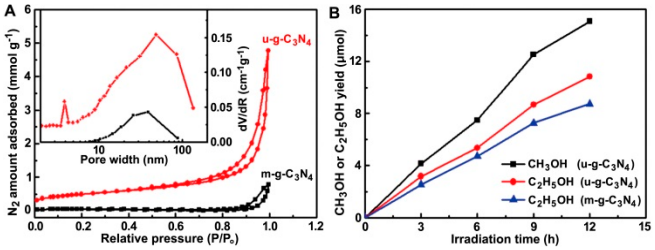

Figure 9. (**A**) N_2 sorption isotherms and Barrett–Joyner–Halenda (BJH) pore size distribution curves (inset) of u-g-C_3N_4 and m-g-C_3N_4. (**B**) The ethanol or methanol yields in the function of irradiation time over u-g-C_3N_4 and m-g-C_3N_4 under visible-light irradiation. Reproduced with permission [102]. Copyright 2013, The Royal Society of Chemistry.

3.2.3. Others

Apart from TiO_2 and g-C_3N_4, some other photocatalysts have also been reported. In a recent report of simultaneously loaded CuO and Pt nanoparticles on reduced $HCa_2Ta_3O_{10}$ perovskite nanosheets for sunlight-driven conversion of CO_2, ethanol was formed as a significant product at a rate of 113 μmol·g^{-1}·h^{-1} [106]. This can be ascribed to their unique structure. Pt nanoparticles with good contact with perovskite nanosheets could serve as excellent trapping sites for photogenerated electrons with a high transfer rate. Meanwhile, the introduction of CuO nanoparticles not only significantly improves the electron–hole separation through the formation of a p–n junction, but also enhances the adsorption of CO_2 and stabilizes C_1 intermediates, thus favoring C-C coupling to form ethanol. In another work, Wang et al. reported the synthesis of $BiVO_4$/RGO nanocomposites for CO_2 photoreduction, which exhibited improved ethanol formation (5.15 μmol·g^{-1}·h^{-1}) in comparison to pure $BiVO_4$ (3.61 μmol·g^{-1}·h^{-1}) [107]. This improvement was attributed to the effective charge transfer of photo-generated electron from $BiVO_4$ to RGO and improved light absorption. In a later study, porous TaON microspheres were synthesized for CO_2 photoreduction via facile nitridation of uniform amorphous Ta_2O_5 sphere formed by hydrothermal treatment [108]. Under the visible light, the conversion of CO_2 to ethanol was improved with a rate of 2.03 μmol·g^{-1}·h^{-1}, which is attributed to the porous spherical architecture of TaON that provided more active sites, enhanced trapping of incident illumination, and promoted charge transfer/separation. Besides this, some other semiconductors, such as Ag@AgBr/CNT [109], red Ag/AgCl [110], $Sr_3Ti_{(2-x-y)}Fe_xS_yO_{(7-z)}N_z$ [111] and $Zn_{0.8}Cd_{0.2}S$ [112], have been used to produce ethanol from photocatalytic CO_2 reduction (Table 3). More effort is still required to improve these photocatalytical systems.

Table 3. Summary of the main photocatalysts with the capability to convert CO_2 into ethanol.

Photocatalyst	Light Source	Reaction Medium	EtOH Yield (μmol·g^{-1}·h^{-1})	Ref.
TiO_2-Rh long nanowires	UV light (λ < 400 nm)	0.5 M Na_2SO_4	12.1	[97]
TiO_2-Pd nanowires	UV light (λ < 400 nm)	0.5 M Na_2SO_4	13	[97]
TiO_2/$Ni(OH)_2$ composite nanofibers	Simulated sunlight	H_2O vapor	0.37	[98]
1.5 wt%Ni^{2+}–TiO_2	UV light (λ < 400 nm)	H_2O vapor	13.2	[99]
5%GQDs/V-TiO_2	Simulated sunlight	8 H_2O mg/L MB and 0.01 M NaOH	5.65	[100]
23.2% AgBr/TiO_2	Visible light λ > 420 nm	0.2 M $KHCO_3$	13.28	[101]
g-C_3N_4 derived from urea	Visible light λ > 420 nm	1.0 M NaOH	4.5	[102]
g-C_3N_4 derived from melamine	Visible light λ > 420 nm	1.0 M NaOH	3.6	[102]

Table 3. *Cont.*

ZnO/g-C_3N_4	Simulated sunlight	H_2O	1.5	[103]
Ag_3PO_4/g-C_3N_4	Simulated sunlight	0.5 M Na_2SO_4	1.3	[104]
5.8wt%Pd/g-C_3N_4	Visible light λ > 420 nm	H_2O vapor	2.18	[105]
Reduced Cu/Pt–$HCa_2Ta_3O_{10}$	Simulated sunlight	H_2O vapor	113	[106]
$BiVO_4$/RGO	Simulated sunlight	0.1 M NaOH	5.15	[107]
TaON microspheres	Visible light λ > 420 nm	1.0 M $NaHCO_3$	2.03	[108]
Ag@AgBr/CNT	Visible light λ > 420 nm	0.2 M $KHCO_3$	2.94	[109]
Red Ag/AgCl	Visible light λ > 420 nm	0.1 M $NaHCO_3$	44.6	[110]
$Sr_3Ti_{(2-x-y)}Fe_xS_yO_{(7-z)}N_z$	UV visible region (300–700 nm)	0.2 M NaOH	9.9	[111]
$Zn_{0.8}Cd_{0.2}S$	Visible light λ > 400 nm	1.0 M $NaHCO_3$	6	[112]

3.3. Photoelectrocatalytic CO_2 Reduction to Ethanol

Photoelectrochemical reduction of CO_2 has been investigated following its first discovery by Halman in 1978 [113]. Employing semiconductors, such as GaP, silicon and CdTe, as the photocathodes [12,14], the conversion of CO_2 into hydrocarbons, especially ethanol, can be realized in the presence of water under illumination and bias potential. In spite of the increasing researches on photoelectroreduction of CO_2 in the last five years, the reports on clean fuel ethanol formation were extremely rare. For instance, a Cu/Cu_2O electrode prepared by electrochemical deposition method catalytically reduces CO_2 to ethanol with the maximum yield of 5.0 ppm in 0.1 mol L^{-1} Na_2CO_3 under the bias potential of 0.2 V vs. Ag/AgCl and UV-Vis irradiation [35]. Equipped with Pt-reduced graphene oxides (RGO)/Cu foam cathode and TiO_2 nanotube photoanode, the phoelectrochemical cell exhibited an ethanol production rate of 105 nmol h^{-1} cm^{-2} under the potential of 2 V and UV-Vis irradiation, which was even significantly higher than that of the simple sum of electrochemical and phochemical processes (82 nmol h^{-1} cm^{-2}) [114], indicating the synergetic effect of electrochemical and phochemical reductions. Importantly, ethanol was observed as the main product over the boron-doped g-C_3N_4 electrodes with or without coupling with Au, Rh or Ag [115]. The yield of ethanol was maximized on boron-doped g-C_3N_4/Au electrode with a value of around 150 nmol under the bias potential of −0.4 V vs. Ag/AgCl and simulated solar irradiation. Afterwards, ZIF-8 was incorporated into Ti/TiO_2 nanotubes electrode to increase the photocurrent, resulting in the ethanol formation of up to 10 mmol L^{-1} under the bias potential of 0.1 V vs. Ag/AgCl and UV-Vis irradiation for three hours (Figure 10) [116]. According to the results mentioned above, highly efficient production of ethanol through photoelectrocatalytic route and even industrialization has a long way to go.

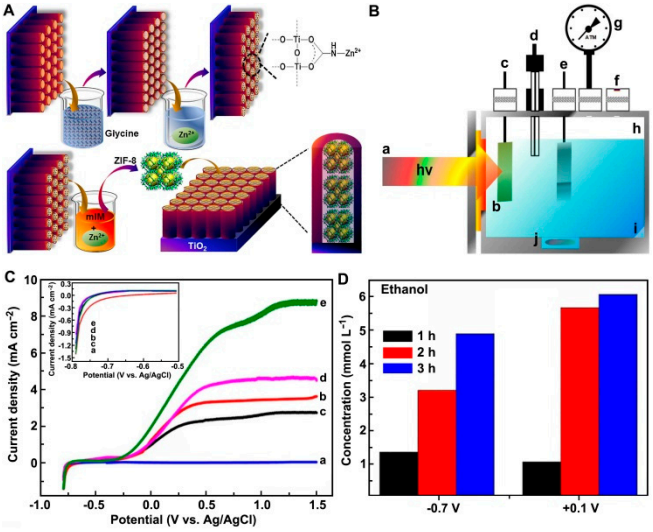

Figure 10. (**A**) Schematic illustration of ZIF-8 formation on Ti/TiO_2NT. (**B**) Photoelectrocatalytic CO_2 reduction reactor used in all experiments: (a) 125W mercury vapor lamp; (b) quartz window; (c) working electrode; (d) reference electrode; (e) counter electrode; (f) septum; (g) manometer; (h) headspace; (i) supporting electrolyte; (j) magnetic bar. (**C**) Linear scanning voltammograms of the electrodes at a scan rate of 10 $mV \cdot s^{-1}$ in 0.1 $mol \cdot L^{-1}$ Na_2SO_4: (a) both electrodes in the dark; (b) Ti/TiO_2NT without CO_2; (c) Ti/TiO_2NT with CO_2; (d) Ti/TiO_2NT-ZIF-8 without CO_2; (e) Ti/TiO_2NT-ZIF-8 with CO_2. (**D**) Concentrations of ethanol generated on Ti/TiO_2NT-ZIF-8 electrode by photoelectrocatalytic CO_2 reduction for 3 h with bias potentials of −0.7 V and +0.1 V vs. Ag/AgCl, in 0.1 $mol \cdot L^{-1}$ Na_2SO_4. Reproduced with permission [116]. Copyright 2018, Elsevier.

4. Conclusions and Perspectives

In conclusion, recent research has indicated the feasibility of producing ethanol from CO_2 by electrochemical, photochemical and photoelectrochemical processes using solar energy and/or renewable electricity over advanced catalysts. Despite the challenges ahead, it is promising to develop highly efficient and economical catalytic systems that use renewable energy to selectively convert CO_2 into clean fuel ethanol over active catalysts in the near future, thus realizing the sustainable development of human beings.

In future studies, more effort should be directed towards the following strategies to boost the performance of electrocatalysts for CO_2-to-ethanol conversion: (1) introducing edges by nanostructuring with cubes, quantum dots, etc., introducing defects by doping and making pores, or introducing grain boundaries by controlled electrochemical growth, into the catalyst surfaces to increase the active sites; (2) designing nanostructured catalysts with special morphologies, such as multi-hollow, core-shell and nanoporous structures, which can confine the CO intermediates for further C–C coupling and ethanol formation; (3) employing metal or nonmetal doping strategies to chemically modify the structures of catalysts; (4) exploring composite materials with synergetic effect as the potential catalysts for CO_2 reduction to realize the cascade reaction; (5) using certain catalysts with high overpotentials towards HER to suppress HER, which would compete electrons with CO_2 electroreduction reaction in the result of low efficiency; (6) incorporating suitable molecular catalysts to reduce the overpotentials of CO_2-to-ethanol conversion by stabilizing the intermediates; (7) designing and optimizing flow cell system using gas-diffusion-electrode to improve the current density to commercially relevant levels; (8) designing catalysts with typical structure models for density functional theory (DFT) calculation and using operando techniques to study the reaction mechanism of CO_2 reduction.

In spite of the great efforts, it still seems quite challenging to efficiently photoreduce CO_2 to desirable products. Although CO_2 could be reduced to ethanol using some certain semiconductor catalysts by photochemical route, the yield and selectivity of ethanol was extremely low and hard to practice on a commercial scale. In the following, several strategies that may promote the ethanol

production from photocatalytic CO_2 reduction are proposed: (1) designing semiconductors with high surface area and porosity to maximize the adsorption of CO_2 and intermediates for further C–C bond formation; (2) coupling two semiconductors with proper band structures for the preferred spatial separation of photo-generated electrons and holes to the electron–hole recombination; (3) introducing oxygen vacancies into semiconductors, which facilitate trapping electrons and activating CO_2; (4) applying a certain amount of external bias voltage to promote the separation of photogenerated electron–hole pairs; (5) deeply understanding the photocatalytic CO_2 reduction process through DFT calculations and advanced in situ techniques for further exploration on highly active catalysts, photoreducing CO_2 to ethanol.

Author Contributions: This work was designed and presented by Y.S. (Yanfang Song), W.C., W.W. and Y.S. (Yuhan Sun). All authors have read and agreed to the published version of the manuscript.

Funding: This work was funded by the National Natural Science Foundation of China (grant number 91745114, 21802160, 21473233), the Ministry of Science and Technology of China (grant number 2016YFA0202800, 2018YFB0604700), Shanghai Sailing Program (grant number 18YF1425700), and the Hundred Talents Program of Chinese Academy of Sciences.

Conflicts of Interest: The authors declare no conflict of interest.

References

1. Duan, X.; Xu, J.; Wei, Z.; Ma, J.; Guo, S.; Wang, S.; Liu, H.; Dou, S. Metal-Free Carbon Materials for CO_2 Electrochemical Reduction. *Adv. Mater.* **2017**, *29*, 1701784. [CrossRef]
2. Vasileff, A.; Zheng, Y.; Qiao, S.Z. Carbon Solving Carbon's Problems: Recent Progress of Nanostructured Carbon-Based Catalysts for the Electrochemical Reduction of CO_2. *Adv. Energy Mater.* **2017**, *7*, 1700759. [CrossRef]
3. Tans, P.; Keeling, R. NORR/ESRL. Available online: http://www.esrl.noaa.gov/gmd/ccgg/trends/ (accessed on 25 May 2020).
4. Li, K.; Peng, B.; Peng, T. Recent advances in heterogeneous photocatalytic CO_2 conversion to solar fuels. *ACS Catal.* **2016**, *6*, 7485–7527. [CrossRef]
5. National Renewable Energy Information Management Platform. Available online: http://djfj.renewable.org.cn/ (accessed on 25 May 2020).
6. Asadi, M.; Kim, K.; Liu, C.; Addepalli, A.V.; Abbasi, P.; Yasaei, P.; Phillips, P.; Behranginia, A.; Cerrato, J.M.; Haasch, R.; et al. Nanostructured transition metal dichalcogenide electrocatalysts for CO_2 reduction in ionic liquid. *Science* **2016**, *353*, 467–470.
7. Gao, S.; Lin, Y.; Jiao, X.; Sun, Y.; Luo, Q.; Zhang, W.; Li, D.; Yang, J.; Xie, Y. Partially oxidized atomic cobalt layers for carbon dioxide electroreduction to liquid fuel. *Nature* **2016**, *529*, 68–71. [CrossRef]
8. Zhang, L.; Zhao, Z.J.; Gong, J. Nanostructured Materials for Heterogeneous Electrocatalytic CO_2 Reduction and Related Reaction Mechanisms. *Angew. Chem. Int. Ed.* **2017**, *56*, 11326–11353. [CrossRef]
9. Habisreutinger, S.N.; Schmidt-Mende, L.; Stolarczyk, J.K. Photocatalytic reduction of CO_2 on TiO_2 and other semiconductors. *Angew. Chem. Int. Ed.* **2013**, *52*, 7372–7408. [CrossRef]
10. Li, Y.; Sun, Q. Recent advances in breaking scaling relations for effective electrochemical conversion of CO_2. *Adv. Energy Mater.* **2016**, *6*, 1600463. [CrossRef]
11. Shih, C.F.; Zhang, T.; Li, J.; Bai, C. Powering the Future with Liquid Sunshine. *Joule* **2018**, *2*, 1925–1949. [CrossRef]
12. Kumar, B.; Llorente, M.; Froehlich, J.; Dang, T.; Sathrum, A.; Kubiak, C.P. Photochemical and photoelectrochemical reduction of CO_2. *Annu. Rev. Phys. Chem.* **2012**, *63*, 541–569. [CrossRef]
13. Jones, J.-P.; Prakash, G.K.S.; Olah, G.A. Electrochemical CO_2 Reduction: Recent Advances and Current Trends. *Isr. J. Chem.* **2014**, *54*, 1451–1466. [CrossRef]
14. Zhao, G.; Huang, X.; Wang, X.; Wang, X. Progress in catalyst exploration for heterogeneous CO_2 reduction and utilization: A critical review. *J. Mater. Chem. A* **2017**, *5*, 21625–21649. [CrossRef]
15. Tu, W.; Zhou, Y.; Zou, Z. Photocatalytic conversion of CO_2 into renewable hydrocarbon fuels: State-of-the-art accomplishment, challenges, and prospects. *Adv. Mater.* **2014**, *26*, 4607–4626. [CrossRef]

16. Tang, Q.; Lee, Y.; Li, D.Y.; Choi, W.; Liu, C.W.; Lee, D.; Jiang, D. Lattice-Hydride Mechanism in Electrocatalytic CO_2 Reduction by Structurally Precise Copper-Hydride Nanoclusters. *J. Am Chem. Soc.* **2017**, *139*, 9728–9736. [CrossRef]
17. Kondratenko, E.V.; Mul, G.; Baltrusaitis, J.; Larrazábal, G.O.; Pérez-Ramírez, J. Status and perspectives of CO_2 conversion into fuels and chemicals by catalytic, photocatalytic and electrocatalytic processes. *Energy Environ. Sci.* **2013**, *6*, 3112. [CrossRef]
18. Zhu, D.D.; Liu, J.L.; Qiao, S.Z. Recent Advances in Inorganic Heterogeneous Electrocatalysts for Reduction of Carbon Dioxide. *Adv. Mater.* **2016**, *28*, 3423–3452. [CrossRef]
19. Lim, R.J.; Xie, M.; Sk, M.A.; Lee, J.-M.; Fisher, A.; Wang, X.; Lim, K.H. A review on the electrochemical reduction of CO_2 in fuel cells, metal electrodes and molecular catalysts. *Catal. Today* **2014**, *233*, 169–180. [CrossRef]
20. Yang, K.D.; Ha, Y.; Sim, U.; An, J.; Lee, C.W.; Jin, K.; Kim, Y.; Park, J.; Hong, J.S.; Lee, J.H.; et al. Graphene Quantum Sheet Catalyzed Silicon Photocathode for Selective CO_2 Conversion to CO. *Adv. Funct. Mater.* **2016**, *26*, 233–242. [CrossRef]
21. Schneider, J.; Jia, H.; Muckerman, J.T.; Fujita, E. Thermodynamics and kinetics of CO_2, CO, and H+ binding to the metal centre of CO_2 reduction catalysts. *Chem. Soc. Rev.* **2012**, *41*, 2036–2051. [CrossRef]
22. Benson, E.E.; Kubiak, C.P.; Sathrum, A.J.; Smieja, J.M. Electrocatalytic and homogeneous approaches to conversion of CO_2 to liquid fuels. *Chem. Soc. Rev.* **2009**, *38*, 89–99. [CrossRef]
23. Burdyny, T.; Smith, W.A. CO_2 reduction on gas-diffusion electrodes and why catalytic performance must be assessed at commercially-relevant conditions. *Energy Environ. Sci.* **2019**, *12*, 1442–1453. [CrossRef]
24. Chen, C.; Khosrowabadi Kotyk, J.F.; Sheehan, S.W. Progress toward Commercial Application of Electrochemical Carbon Dioxide Reduction. *Chem* **2018**, *4*, 2571–2586. [CrossRef]
25. Zhang, J.; Luo, W.; Züttel, A. Self-supported copper-based gas diffusion electrodes for CO_2 electrochemical reduction. *J. Mater. Chem. A* **2019**, *7*, 26285–26292. [CrossRef]
26. Mao, J.; Li, K.; Peng, T. Recent advances in the photocatalytic CO_2 reduction over semiconductors. *Catal. Sci. Technol.* **2013**, *3*, 2481–2498. [CrossRef]
27. Li, K.; An, X.; Park, K.H.; Khraisheh, M.; Tang, J. A critical review of CO_2 photoconversion: Catalysts and reactors. *Catal. Today* **2014**, *224*, 3–12. [CrossRef]
28. Das, S.; Wan Daud, W.M.A. A review on advances in photocatalysts towards CO_2 conversion. *RSC Adv.* **2014**, *4*, 20856. [CrossRef]
29. Corma, A.; Garcia, H. Photocatalytic reduction of CO_2 for fuel production: Possibilities and challenges. *J. Catal.* **2013**, *308*, 168–175. [CrossRef]
30. Van Gerven, T.; Mul, G.; Moulijn, J.; Stankiewicz, A. A review of intensification of photocatalytic processes. *Chem. Eng. Process.* **2007**, *46*, 781–789. [CrossRef]
31. Tahir, M.; Amin, N.S. Advances in visible light responsive titanium oxide-based photocatalysts for CO_2 conversion to hydrocarbon fuels. *Energy Convers. Manag.* **2013**, *76*, 194–214. [CrossRef]
32. Chang, X.; Wang, T.; Gong, J. CO_2 photo-reduction: Insights into CO_2 activation and reaction on surfaces of photocatalysts. *Energy Environ. Sci.* **2016**, *9*, 2177–2196. [CrossRef]
33. Ran, J.; Jaroniec, M.; Qiao, S.Z. Cocatalysts in semiconductor-based photocatalytic CO_2 reduction: Achievements, challenges, and opportunities. *Adv. Mater.* **2018**, *30*, 1704649. [CrossRef] [PubMed]
34. Barton, E.E.; Rampulla, D.M.; Bocarsly, A.B. Selective solar-driven reduction of CO_2 to methanol using a catalyzed p-GaP based photoelectrochemical cell. *J. Am. Chem. Soc.* **2008**, *130*, 6342–6344. [CrossRef]
35. Ba, X.; Yan, L.-L.; Huang, S.; Yu, J.; Xia, X.-J.; Yu, Y. New Way for CO_2 Reduction under Visible Light by a Combination of a Cu Electrode and Semiconductor Thin Film: Cu_2O Conduction Type and Morphology Effect. *J. Phys. Chem. C* **2014**, *118*, 24467–24478. [CrossRef]
36. Arai, T.; Sato, S.; Kajino, T.; Morikawa, T. Solar CO_2 reduction using H_2O by a semiconductor/metal-complex hybrid photocatalyst: Enhanced efficiency and demonstration of a wireless system using $SrTiO_3$ photoanodes. *Energy Environ. Sci.* **2013**, *6*, 1274–1282. [CrossRef]
37. Ganesh, I. Conversion of carbon dioxide into methanol–a potential liquid fuel: Fundamental challenges and opportunities (a review). *Renew. Sustain. Energy Rev.* **2014**, *31*, 221–257. [CrossRef]
38. Indrakanti, V.P.; Kubicki, J.D.; Schobert, H.H. Photoinduced activation of CO_2 on Ti-based heterogeneous catalysts: Current state, chemical physics-based insights and outlook. *Energy Environ. Sci.* **2009**, *2*, 745–758. [CrossRef]

39. Indrakanti, V.P.; Schobert, H.H.; Kubicki, J.D. Quantum Mechanical Modeling of CO_2 Interactions with Irradiated Stoichiometric and Oxygen-Deficient Anatase TiO_2 Surfaces: Implications for the Photocatalytic Reduction of CO_2. *Energy Fuels* **2009**, *23*, 5247–5256. [CrossRef]
40. Kortlever, R.; Shen, J.; Schouten, K.J.P.; Calle-Vallejo, F.; Koper, M.T.M. Catalysts and Reaction Pathways for the Electrochemical Reduction of Carbon Dioxide. *J. Phys. Chem. Lett.* **2015**, *6*, 4073–4082. [CrossRef]
41. Song, Y.; Peng, R.; Hensley, D.K.; Bonnesen, P.V.; Liang, L.; Wu, Z.; Meyer, H.M.; Chi, M.; Ma, C.; Sumpter, B.G.; et al. High-Selectivity Electrochemical Conversion of CO_2 to Ethanol using a Copper Nanoparticle/N-Doped Graphene Electrode. *ChemistrySelect* **2016**, *1*, 6055–6061. [CrossRef]
42. Peterson, A.A.; Abild-Pedersen, F.; Studt, F.; Rossmeisl, J.; Norskov, J.K. How copper catalyzes the electroreduction of carbon dioxide into hydrocarbon fuels. *Energy Environ. Sci.* **2010**, *3*, 1311–1315. [CrossRef]
43. Calle-Vallejo, F.; Koper, M.T. Theoretical considerations on the electroreduction of CO to C_2 species on Cu(100) electrodes. *Angew. Chem. Int. Ed.* **2013**, *52*, 7282–7285. [CrossRef]
44. Ren, D.; Ang, B.S.-H.; Yeo, B.S. Tuning the Selectivity of Carbon Dioxide Electroreduction toward Ethanol on Oxide-Derived Cu_xZn Catalysts. *ACS Catal.* **2016**, *6*, 8239–8247. [CrossRef]
45. Ren, D.; Deng, Y.; Handoko, A.D.; Chen, C.S.; Malkhandi, S.; Yeo, B.S. Selective Electrochemical Reduction of Carbon Dioxide to Ethylene and Ethanol on Copper(I) Oxide Catalysts. *ACS Catal.* **2015**, *5*, 2814–2821. [CrossRef]
46. Yin, Z.; Yu, C.; Zhao, Z.; Guo, X.; Shen, M.; Li, N.; Muzzio, M.; Li, J.; Liu, H.; Lin, H.; et al. Cu_3N Nanocubes for Selective Electrochemical Reduction of CO_2 to Ethylene. *Nano Lett.* **2019**, *19*, 8658–8663. [CrossRef]
47. De Brito, J.F.; Araujo, A.R.; Rajeshwar, K.; Zanoni, M.V.B. Photoelectrochemical reduction of CO_2 on Cu/Cu_2O films: Product distribution and pH effects. *Chem. Eng. J.* **2015**, *264*, 302–309. [CrossRef]
48. Teeter, T.E.; Van Rysselberghe, P. Reduction of Carbon Dioxide on Mercury Cathodes. *J. Chem. Phys.* **1954**, *22*, 759–760. [CrossRef]
49. Zhang, S.; Fan, Q.; Xia, R.; Meyer, T.J. CO_2 reduction: From homogeneous to heterogeneous electrocatalysis. *Acc. Chem. Res.* **2020**, *53*, 255–264. [CrossRef]
50. Nitopi, S.; Bertheussen, E.; Scott, S.B.; Liu, X.; Engstfeld, A.K.; Horch, S.; Seger, B.; Stephens, I.E.L.; Chan, K.; Hahn, C.; et al. Progress and Perspectives of Electrochemical CO_2 Reduction on Copper in Aqueous Electrolyte. *Chem. Rev.* **2019**. [CrossRef]
51. Popovic, S.; Smiljanic, M.; Jovanovic, P.; Vavra, J.; Buonsanti, R.; Hodnik, N. Stability and degradation mechanisms of copper-based catalysts for electrochemical CO_2 reduction. *Angew. Chem. Int. Ed.* **2020**. [CrossRef]
52. Ma, M.; Djanashvili, K.; Smith, W.A. Controllable Hydrocarbon Formation from the Electrochemical Reduction of CO_2 over Cu Nanowire Arrays. *Angew. Chem. Int. Ed.* **2016**, *55*, 6680–6684. [CrossRef]
53. Lv, J.J.; Jouny, M.; Luc, W.; Zhu, W.; Zhu, J.J.; Jiao, F. A Highly Porous Copper Electrocatalyst for Carbon Dioxide Reduction. *Adv. Mater.* **2018**, *30*, e1803111. [CrossRef]
54. Lum, Y.; Yue, B.; Lobaccaro, P.; Bell, A.T.; Ager, J.W. Optimizing C–C Coupling on Oxide-Derived Copper Catalysts for Electrochemical CO_2 Reduction. *J. Phys. Chem. C* **2017**, *121*, 14191–14203. [CrossRef]
55. De Luna, P.; Quintero-Bermudez, R.; Dinh, C.-T.; Ross, M.B.; Bushuyev, O.S.; Todorović, P.; Regier, T.; Kelley, S.O.; Yang, P.; Sargent, E.H. Catalyst electro-redeposition controls morphology and oxidation state for selective carbon dioxide reduction. *Nat. Catal.* **2018**, *1*, 103–110. [CrossRef]
56. Loiudice, A.; Lobaccaro, P.; Kamali, E.A.; Thao, T.; Huang, B.H.; Ager, J.W.; Buonsanti, R. Tailoring Copper Nanocrystals towards C_2 Products in Electrochemical CO_2 Reduction. *Angew. Chem. Int. Ed.* **2016**, *55*, 5789–5792. [CrossRef]
57. Jiang, K.; Sandberg, R.B.; Akey, A.J.; Liu, X.; Bell, D.C.; Nørskov, J.K.; Chan, K.; Wang, H. Metal ion cycling of Cu foil for selective C–C coupling in electrochemical CO_2 reduction. *Nat. Catal.* **2018**, *1*, 111–119. [CrossRef]
58. Chen, Z.; Wang, T.; Liu, B.; Cheng, D.; Hu, C.; Zhang, G.; Zhu, W.; Wang, H.; Zhao, Z.J.; Gong, J. Grain-Boundary-Rich Copper for Efficient Solar-Driven Electrochemical CO_2 Reduction to Ethylene and Ethanol. *J. Am. Chem.Soc.* **2020**, *142*, 6878–6883. [CrossRef]
59. Zhu, Q.; Sun, X.; Yang, D.; Ma, J.; Kang, X.; Zheng, L.; Zhang, J.; Wu, Z.; Han, B. Carbon dioxide electroreduction to C_2 products over copper-cuprous oxide derived from electrosynthesized copper complex. *Nat. Commun.* **2019**, *10*, 3851. [CrossRef]

60. Yang, P.P.; Zhang, X.L.; Gao, F.Y.; Zheng, Y.R.; Niu, Z.Z.; Yu, X.; Liu, R.; Wu, Z.Z.; Qin, S.; Chi, L.P.; et al. Protecting Copper Oxidation State via Intermediate Confinement for Selective CO_2 Electroreduction to C_{2+} Fuels. *J. Am. Chem. Soc.* **2020**, *142*, 6400–6408. [CrossRef] [PubMed]
61. Liang, Z.Q.; Zhuang, T.T.; Seifitokaldani, A.; Li, J.; Huang, C.W.; Tan, C.S.; Li, Y.; De Luna, P.; Dinh, C.T.; Hu, Y.; et al. Copper-on-nitride enhances the stable electrosynthesis of multi-carbon products from CO_2. *Nat. Commun.* **2018**, *9*, 3828. [CrossRef]
62. Chen, C.; Sun, X.; Lu, L.; Yang, D.; Ma, J.; Zhu, Q.; Qian, Q.; Han, B. Efficient electroreduction of CO_2 to C_2 products over B-doped oxide-derived copper. *Green Chem.* **2018**, *20*, 4579–4583. [CrossRef]
63. Zhou, Y.; Che, F.; Liu, M.; Zou, C.; Liang, Z.; De Luna, P.; Yuan, H.; Li, J.; Wang, Z.; Xie, H.; et al. Dopant-induced electron localization drives CO_2 reduction to C_2 hydrocarbons. *Nat. Chem.* **2018**, *10*, 974–980. [CrossRef]
64. Zhuang, T.-T.; Liang, Z.-Q.; Seifitokaldani, A.; Li, Y.; De Luna, P.; Burdyny, T.; Che, F.; Meng, F.; Min, Y.; Quintero-Bermudez, R.; et al. Steering post-C–C coupling selectivity enables high efficiency electroreduction of carbon dioxide to multi-carbon alcohols. *Nat. Catal.* **2018**, *1*, 421–428. [CrossRef]
65. Ma, W.; Xie, S.; Liu, T.; Fan, Q.; Ye, J.; Sun, F.; Jiang, Z.; Zhang, Q.; Cheng, J.; Wang, Y. Electrocatalytic reduction of CO_2 to ethylene and ethanol through hydrogen-assisted C–C coupling over fluorine-modified copper. *Nat. Catal.* **2020**. [CrossRef]
66. Luo, M.; Wang, Z.; Li, Y.C.; Li, J.; Li, F.; Lum, Y.; Nam, D.H.; Chen, B.; Wicks, J.; Xu, A.; et al. Hydroxide promotes carbon dioxide electroreduction to ethanol on copper via tuning of adsorbed hydrogen. *Nat. Commun.* **2019**, *10*, 5814. [CrossRef]
67. Han, Z.; Kortlever, R.; Chen, H.Y.; Peters, J.C.; Agapie, T. CO_2 Reduction Selective for $C_{\geq 2}$ Products on Polycrystalline Copper with N-Substituted Pyridinium Additives. *ACS Cent. Sci.* **2017**, *3*, 853–859. [CrossRef]
68. Thevenon, A.; Rosas-Hernandez, A.; Peters, J.C.; Agapie, T. In-Situ Nanostructuring and Stabilization of Polycrystalline Copper by an Organic Salt Additive Promotes Electrocatalytic CO_2 Reduction to Ethylene. *Angew. Chem. Int. Ed.* **2019**, *58*, 16952–16958. [CrossRef]
69. Wakerley, D.; Lamaison, S.; Ozanam, F.; Menguy, N.; Mercier, D.; Marcus, P.; Fontecave, M.; Mougel, V. Bio-inspired hydrophobicity promotes CO_2 reduction on a Cu surface. *Nat. Mater.* **2019**, *18*, 1222–1227. [CrossRef]
70. Li, F.; Li, Y.C.; Wang, Z.; Li, J.; Nam, D.-H.; Lum, Y.; Luo, M.; Wang, X.; Ozden, A.; Hung, S.-F.; et al. Cooperative CO_2-to-ethanol conversion via enriched intermediates at molecule–metal catalyst interfaces. *Nat. Catal.* **2019**, *3*, 75–82. [CrossRef]
71. Jia, F.; Yu, X.; Zhang, L. Enhanced selectivity for the electrochemical reduction of CO_2 to alcohols in aqueous solution with nanostructured Cu–Au alloy as catalyst. *J. Power Sources* **2014**, *252*, 85–89. [CrossRef]
72. Ishimaru, S.; Shiratsuchi, R.; Nogami, G. Pulsed Electroreduction of CO_2 on Cu-Ag Alloy Electrodes. *J. Electrochem. Soc.* **2000**, *147*, 1864. [CrossRef]
73. Hoang, T.T.H.; Verma, S.; Ma, S.; Fister, T.T.; Timoshenko, J.; Frenkel, A.I.; Kenis, P.J.A.; Gewirth, A.A. Nanoporous Copper-Silver Alloys by Additive-Controlled Electrodeposition for the Selective Electroreduction of CO_2 to Ethylene and Ethanol. *J. Am. Chem. Soc.* **2018**, *140*, 5791–5797. [CrossRef]
74. Dutta, A.; Montiel, I.Z.; Erni, R.; Kiran, K.; Rahaman, M.; Drnec, J.; Broekmann, P. Activation of bimetallic AgCu foam electrocatalysts for ethanol formation from CO_2 by selective Cu oxidation/reduction. *Nano Energy* **2020**, *68*. [CrossRef]
75. Ma, S.; Sadakiyo, M.; Heima, M.; Luo, R.; Haasch, R.T.; Gold, J.I.; Yamauchi, M.; Kenis, P.J. Electroreduction of Carbon Dioxide to Hydrocarbons Using Bimetallic Cu-Pd Catalysts with Different Mixing Patterns. *J. Am. Chem. Soc.* **2017**, *139*, 47–50. [CrossRef] [PubMed]
76. Ren, D.; Gao, J.; Pan, L.; Wang, Z.; Luo, J.; Zakeeruddin, S.M.; Hagfeldt, A.; Grätzel, M. Atomic Layer Deposition of ZnO on CuO Enables Selectiveand Efficient Electroreduction of Carbon Dioxide to Liquid Fuels. *Angew. Chem. Int. Ed.* **2019**, *58*, 15036–15040. [CrossRef]
77. Jung, H.; Lee, S.Y.; Lee, C.W.; Cho, M.K.; Won, D.H.; Kim, C.; Oh, H.S.; Min, B.K.; Hwang, Y.J. Electrochemical Fragmentation of Cu_2O Nanoparticles Enhancing Selective C-C Coupling from CO_2 Reduction Reaction. *J. Am. Chem. Soc.* **2019**, *141*, 4624–4633. [CrossRef]
78. Zhao, K.; Liu, Y.; Quan, X.; Chen, S.; Yu, H. CO_2 Electroreduction at Low Overpotential on Oxide-Derived Cu/Carbons Fabricated from Metal Organic Framework. *ACS Appl. Mater. Interfaces* **2017**, *9*, 5302–5311. [CrossRef]

79. Han, H.; Noh, Y.; Kim, Y.; Park, S.; Yoon, W.; Jang, D.; Choi, S.M.; Kim, W.B. Selective electrochemical CO_2 conversion to multicarbon alcohols on highly efficient N-doped porous carbon-supported Cu catalysts. *Green Chem.* **2020**, *22*, 71–84. [CrossRef]
80. Wu, J.; Ma, S.; Sun, J.; Gold, J.I.; Tiwary, C.; Kim, B.; Zhu, L.; Chopra, N.; Odeh, I.N.; Vajtai, R.; et al. A metal-free electrocatalyst for carbon dioxide reduction to multi-carbon hydrocarbons and oxygenates. *Nat. Commun.* **2016**, *7*, 13869. [CrossRef]
81. Song, Y.; Chen, W.; Zhao, C.; Li, S.; Wei, W.; Sun, Y. Metal-Free Nitrogen-Doped Mesoporous Carbon for Electroreduction of CO_2 to Ethanol. *Angew. Chem. Int. Ed.* **2017**, *56*, 10840–10844. [CrossRef] [PubMed]
82. Song, Y.; Wang, S.; Chen, W.; Li, S.; Feng, G.; Wei, W.; Sun, Y. Enhanced Ethanol Production from CO_2 Electroreduction at Micropores in Nitrogen-Doped Mesoporous Carbon. *ChemSusChem* **2020**, *13*, 293–297. [CrossRef]
83. Liu, Y.; Zhang, Y.; Cheng, K.; Quan, X.; Fan, X.; Su, Y.; Chen, S.; Zhao, H.; Zhang, Y.; Yu, H.; et al. Selective electrochemical reduction of CO_2 to ethanol on B and N codoped nanodiamond. *Angew. Chem. Int. Ed.* **2017**, *56*, 15607–15611. [CrossRef]
84. Reller, C.; Krause, R.; Volkova, E.; Schmid, B.; Neubauer, S.; Rucki, A.; Schuster, M.; Schmid, G. Selective Electroreduction of CO_2 toward Ethylene on Nano Dendritic Copper Catalysts at High Current Density. *Adv. Energy Mater.* **2017**. [CrossRef]
85. Li, C.W.; Kanan, M.W. CO_2 reduction at low overpotential on Cu electrodes resulting from the reduction of thick Cu_2O films. *J. Am. Chem. Soc.* **2012**, *134*, 7231–7234. [CrossRef]
86. Handoko, A.D.; Chan, K.W.; Yeo, B.S. $–CH_3$ Mediated Pathway for the Electroreduction of CO_2 to Ethane and Ethanol on Thick Oxide-Derived Copper Catalysts at Low Overpotentials. *ACS Energy Lett.* **2017**, *2*, 2103–2109. [CrossRef]
87. Lei, Q.; Zhu, H.; Song, K.; Wei, N.; Liu, L.; Zhang, D.; Yin, J.; Dong, X.; Yao, K.; Wang, N.; et al. Investigating the Origin of Enhanced C_{2+} Selectivity in Oxide-/Hydroxide-Derived Copper Electrodes during CO_2 Electroreduction. *J. Am. Chem. Soc.* **2020**, *142*, 4213–4222. [CrossRef]
88. Nam, D.H.; De Luna, P.; Rosas-Hernandez, A.; Thevenon, A.; Li, F.; Agapie, T.; Peters, J.C.; Shekhah, O.; Eddaoudi, M.; Sargent, E.H. Molecular enhancement of heterogeneous CO_2 reduction. *Nat. Mater.* **2020**, *19*, 266–276. [CrossRef]
89. Vasileff, A.; Xu, C.; Jiao, Y.; Zheng, Y.; Qiao, S.-Z. Surface and Interface Engineering in Copper-Based Bimetallic Materials for Selective CO_2 Electroreduction. *Chem* **2018**, *4*, 1809–1831. [CrossRef]
90. Lee, C.W.; Yang, K.D.; Nam, D.H.; Jang, J.H.; Cho, N.H.; Im, S.W.; Nam, K.T. Defining a materials database for the design of copper binary alloy catalysts for electrochemical CO_2 conversion. *Adv. Mater.* **2018**, *30*. [CrossRef] [PubMed]
91. Albo, J.; Vallejo, D.; Beobide, G.; Castillo, O.; Castano, P.; Irabien, A. Copper-Based Metal-Organic Porous Materials for CO_2 Electrocatalytic Reduction to Alcohols. *ChemSusChem* **2017**, *10*, 1100–1109. [CrossRef]
92. Vu, N.N.; Kaliaguine, S.; Do, T.O. Critical Aspects and Recent Advances in Structural Engineering of Photocatalysts for Sunlight-Driven Photocatalytic Reduction of CO_2 into Fuels. *Adv. Funct. Mater.* **2019**, *29*. [CrossRef]
93. Whang, D.R.; Apaydin, D.H. Artificial Photosynthesis: Learning from Nature. *ChemPhotoChem* **2018**, *2*, 148–160. [CrossRef]
94. Zhao, T.-T.; Feng, G.-H.; Chen, W.; Song, Y.-F.; Dong, X.; Li, G.-H.; Zhang, H.-J.; Wei, W. Artificial bioconversion of carbon dioxide. *Chin. J. Catal.* **2019**, *40*, 1421–1437. [CrossRef]
95. Zhang, Y.; Xia, B.; Ran, J.; Davey, K.; Qiao, S.Z. Atomic-Level Reactive Sites for Semiconductor-Based Photocatalytic CO_2 Reduction. *Adv. Energy Mater.* **2020**, *10*. [CrossRef]
96. Liu, L.; Wang, S.; Huang, H.; Zhang, Y.; Ma, T. Surface sites engineering on semiconductors to boost photocatalytic CO_2 reduction. *Nano Energy* **2020**, *75*. [CrossRef]
97. Zhu, Y.; Xu, Z.; Lang, Q.; Jiang, W.; Yin, Q.; Zhong, S.; Bai, S. Grain boundary engineered metal nanowire cocatalysts for enhanced photocatalytic reduction of carbon dioxide. *Appl. Catal. B Environ.* **2017**, *206*, 282–292. [CrossRef]
98. Meng, A.; Wu, S.; Cheng, B.; Yu, J.; Xu, J. Hierarchical $TiO_2/Ni(OH)_2$ composite fibers with enhanced photocatalytic CO_2 reduction performance. *J. Mater. Chem. A* **2018**, *6*, 4729–4736. [CrossRef]
99. Ola, O.; Mercedes Maroto-Valer, M. Role of catalyst carriers in CO_2 photoreduction over nanocrystalline nickel loaded TiO_2-based photocatalysts. *J. Catal.* **2014**, *309*, 300–308. [CrossRef]

100. Zou, J.-P.; Wu, D.-D.; Luo, J.; Xing, Q.-J.; Luo, X.-B.; Dong, W.-H.; Luo, S.-L.; Du, H.-M.; Suib, S.L. A Strategy for One-Pot Conversion of Organic Pollutants into Useful Hydrocarbons through Coupling Photodegradation of MB with Photoreduction of CO_2. *ACS Catal.* **2016**, *6*, 6861–6867. [CrossRef]
101. Abou Asi, M.; He, C.; Su, M.; Xia, D.; Lin, L.; Deng, H.; Xiong, Y.; Qiu, R.; Li, X.-Z. Photocatalytic reduction of CO_2 to hydrocarbons using AgBr/TiO_2 nanocomposites under visible light. *Catal. Today* **2011**, *175*, 256–263. [CrossRef]
102. Mao, J.; Peng, T.; Zhang, X.; Li, K.; Ye, L.; Zan, L. Effect of graphitic carbon nitride microstructures on the activity and selectivity of photocatalytic CO_2 reduction under visible light. *Catal. Sci. Technol.* **2013**, *3*, 1253. [CrossRef]
103. He, Y.; Wang, Y.; Zhang, L.; Teng, B.; Fan, M. High-efficiency conversion of CO_2 to fuel over ZnO/g-C_3N_4 photocatalyst. *Appl. Catal. B Environ.* **2015**, *168*, 1–8. [CrossRef]
104. He, Y.; Zhang, L.; Teng, B.; Fan, M. New application of Z-scheme Ag_3PO_4/g-C_3N_4 composite in converting CO_2 to fuel. *Environ. Sci. Technol.* **2015**, *49*, 649–656. [CrossRef] [PubMed]
105. Bai, S.; Wang, X.; Hu, C.; Xie, M.; Jiang, J.; Xiong, Y. Two-dimensional g-C_3N_4: An ideal platform for examining facet selectivity of metal co-catalysts in photocatalysis. *Chem. Commun.* **2014**, *50*, 6094–6097. [CrossRef]
106. Vu, N.-N.; Nguyen, C.-C.; Kaliaguine, S.; Do, T.-O. Reduced Cu/Pt-$HCa_2Ta_3O_{10}$ Perovskite Nanosheets for Sunlight-Driven Conversion of CO_2 into Valuable Fuels. *Adv. Sustain. Syst.* **2017**, *1*. [CrossRef]
107. Wang, A.; Shen, S.; Zhao, Y.; Wu, W. Preparation and characterizations of $BiVO_4$/reduced graphene oxide nanocomposites with higher visible light reduction activities. *J. Colloid Interface Sci.* **2015**, *445*, 330–336. [CrossRef]
108. Han, Q.; Zhou, Y.; Tang, L.; Li, P.; Tu, W.; Li, L.; Li, H.; Zou, Z. Synthesis of single-crystalline, porous TaON microspheres toward visible-light photocatalytic conversion of CO_2 into liquid hydrocarbon fuels. *RSC Adv.* **2016**, *6*, 90792–90796. [CrossRef]
109. Abou Asi, M.; Zhu, L.; He, C.; Sharma, V.K.; Shu, D.; Li, S.; Yang, J.; Xiong, Y. Visible-light-harvesting reduction of CO_2 to chemical fuels with plasmonic Ag@AgBr/CNT nanocomposites. *Catal. Today* **2013**, *216*, 268–275. [CrossRef]
110. Cai, B.; Wang, J.; Gan, S.; Han, D.; Wu, Z.; Niu, L. A distinctive red Ag/AgCl photocatalyst with efficient photocatalytic oxidative and reductive activities. *J. Mater. Chem. A* **2014**, *2*, 5280–5286. [CrossRef]
111. Jeyalakshmi, V.; Mahalakshmy, R.; Krishnamurthy, K.R.; Viswanathan, B. Strontium titanates with perovskite structure as photo catalysts for reduction of CO_2 by water: Influence of co-doping with N, S & Fe. *Catal. Today* **2018**, *300*, 152–159. [CrossRef]
112. Tang, L.; Kuai, L.; Li, Y.; Li, H.; Zhou, Y.; Zou, Z. $Zn_xCd_{1-x}S$ tunable band structure-directing photocatalytic activity and selectivity of visible-light reduction of CO_2 into liquid solar fuels. *Nanotechnology* **2018**, *29*. [CrossRef]
113. Halmann, M. Photoelectrochemical reduction of aqueous carbon dioxide on p-type gallium phosphide in liquid junction solar cells. *Nature* **1978**, *275*, 115–116. [CrossRef]
114. Cheng, J.; Zhang, M.; Wu, G.; Wang, X.; Zhou, J.; Cen, K. Photoelectrocatalytic Reduction of CO_2 into Chemicals Using Pt-Modified Reduced Graphene Oxide Combined with Pt-Modified TiO_2 Nanotubes. *Environ. Sci. Technol.* **2014**, *48*, 7076–7084. [CrossRef]
115. Sagara, N.; Kamimura, S.; Tsubota, T.; Ohno, T. Photoelectrochemical CO_2 reduction by a p-type boron-doped g-C_3N_4 electrode under visible light. *Appl. Catal. B Environ.* **2016**, *192*, 193–198. [CrossRef]
116. Cardoso, J.C.; Stulp, S.; de Brito, J.F.; Flor, J.B.S.; Frem, R.C.G.; Zanoni, M.V.B. MOFs based on ZIF-8 deposited on TiO_2 nanotubes increase the surface adsorption of CO_2 and its photoelectrocatalytic reduction to alcohols in aqueous media. *Appl. Catal. B Environ.* **2018**, *225*, 563–573. [CrossRef]